CHAPTER SIX: THE ST. BERNARD AND LOWER NINTH WARD PROTECTED AREA

6.1 Introduction

As described previously in Chapter 2, St. Bernard Parish and the Lower Ninth Ward are protected by a single continuous "ring" of levees that, together, constitute one of the three main protected basins flooded by hurricane Katrina.

Figures 2.11 and 6.1 show the locations of the principal breaches and distressed sections of the levee and floodwall system protecting this basin. Figure 6.2 shows the inundation of this basin four days after the hurricane, on September 2, 2005. At the time shown in this figure, the floodwaters have been partially drained out from the flooded basin, and they are shown at elevation + 3 feet (MSL) [or +5 feet, NAVD 88.]

Cloud cover obstructed the taking of a good image of the flooding at its peak, but this basin flooded very rapidly in the first hours of the main storm surge. The levees were massively breached and catastrophically eroded on the northeastern flank; fronting the MRGO channel and Lake Borgne. In addition, two large breaches occurred at the west end of this protected basin, fronting the IHNC. The result was that this basin flooded extremely rapidly, before the storm surge had subsided, and the resulting surge-pushed floodwaters rose to an elevation of approximately + 12 feet above mean sea level in this basin. As a result, even homes and businesses located on ground well above sea level were inundated. Of course, sites on lower ground were inundated to greater depths.

After the hurricane passed, and the storm surge had subsided, a number of "notches" were deliberately excavated through several of the levees to facilitate drainage of ponded floodwaters by simple gravity flow (as indicated by the yellow stars in Figure 6.1).

6.2 The Northeast Frontage Levees

As shown in Figures 2.9 through 2.11, the initial storm surge swelled the waters of "Lake" Borgne (which is actually a bay, as it is connected directly to the Gulf of Mexico.) As the eye of the hurricane then continued to the north, the counterclockwise swirl of the winds pushed the elevated waters of Lake Borgne to the west, against the levees along the northeast frontage of the St. Bernard protected basin. The result was catastrophic erosion of the levees along much of this frontage, and the through-passage of the floodwaters.

Figures 6.3 and 6.4 show two sections of the levees along this frontage after this event. These are aerial views taken from significant elevation, and they each show many hundreds of feet of levee section that have been catastrophically eroded. In Figure 6.3, the depression in the foundation soils induced by the settlement of the now-vanished levee, and the erosion produced by the turbulent flow across the original levee footprint, is the only sign of the former presence of a levee. In Figure 6.4, a sheetpile curtain had been driven along the centerline of the levee crest, to raise a section that had settled as an interim measure until the

final stage of fill placement could re-raise this embankment section to the final design grade. The levee embankment has eroded completely from both sides of these sheetpiles, and the large diameter pipe in this figure was resting on the crest and slopes of the now vanished levee and so serves as a visual template to show the size and shape (the outline) of the levee section that is now gone.

Figure 6.5 shows another view of massive erosion along a long stretch of levees along this "MRGO frontage" section, this time a bit farther to the south (nearer to the second navigational lock structure at bayou Dupres.) Here the massive erosion is not as complete, and portions of the levee embankment remain. In this photo, the eroded detritus can be clearly seen to be strewn back behind the partially eroded levees, and the sandy (and shell sand) nature of some of this eroded material is evident.

Figure 6.6 shows a ground level view of the sheetpiles from Figure 6.4. In this photo it can be clearly seen that the sheetpiles, which had originally been driven to constant grade, have settled differentially under the pounding of the storm surge and storm driven waves. This would suggest that the cyclic wave loading may have caused pore pressure increases in the fine, sandy foundation soils into which the sheetpiles were embedded, and that this (full or partial) liquefaction reduced the bearing strength and stiffness of these foundation soils and led to the observed differential sheetpile settlements as the sheetpiles were only lightly self-loaded with regard to vertical bearing and settlements.

LIDAR surveys were performed by the USACE to document the elevation of the levee crest along the full 11-mile long northeast (MRGO) frontage both before and after Katrina. An example is shown in Figure 6.7, where the magenta line indicates the crest elevation prior to Katrina, and the darker blue line indicates the crest elevation afterwards. The photo at the top of this figure is a vertical (plan view) photographic image along the same section. The two LIDAR surveys serve to show the amount of erosion-induced crest loss along this section, and this can be correlated with the same locations in the photo at the top. Note the light material streamed back behind the levees (on the "protected side") in the corresponding photo; representing eroded material from the levees strewn back into the inboard side swamps.

Figure 6.7 includes the large (gated) reinforced concrete navigation control structure at Bayou Bienvenue. A large barge was deposited on the crest of the levee immediately to the north of this lock structure, and this can be clearly seen in Figure 6.7. Figure 6.8 shows a second view, of the massive breach eroded at the contact between the lock structure and the adjacent levee embankment.

Figure 6.9(a) is an oblique aerial of the smaller Bayou Dupres concrete navigation structure situated farther to the south along this same MRGO levee frontage, showing a similar massive eroded breach at the juncture between the northwest end of the concrete structure and the adjoining earthen levee section. Figure 6.9(b) shows a second view, taken from the eroded breach and looking to the inboard (protected) side along the north flank of Bayou Dupres, showing the eroded detritus strewn inland from this breach. In this figure, it can be clearly seen that large fractions of the eroded material consisted of shell sand fill. The use of lightweight shell sand fill had been called for at this interface section in order to

minimize differential settlements between the embankment section and the adjacent concrete lock structure. By minimizing these differential settlements, the formation of a small settlement-induced gap between the levee and the lock structure would be prevented. As a result of using the dangerously erodeable lightweight shell sand fill, however, a massive eroded breach occurred instead.

The crest heights of the levees along much of this MRGO frontage section were several feet below design grade at the time of Katrina's arrival. This levee frontage was being constructed in stages, to allow time for settlement of the evolving levees and for dissipation of pore pressures (which results in progressive strength and stiffness gain in both the levee fill and in the underlying foundation soils, so that the softer foundation soils can safely support the increasing levee section height and weight of the next stage.) The USACE had reportedly long requested appropriation of the funds necessary to place the final stage of fill and bring this critical 11-mile long section up to full design grade. That funding did not arrive in time.

The levees along this frontage were unusually vulnerable to erosion as they were "sand core" levees, constructed largely using material available from the adjacent MRGO channel excavation. Given the nature of the local soils at this location, much of that excavated material consisted of sands and lightweight shell sands. These materials have a low intrinsic resistance to erosion (see Chapters 9 and 10), and this led to a hazardous condition. It is possible that the final fill stage, if it had arrived in time, might have provided a covering veneer of compacted clay fill (with a higher resistance to erosion), but such a covering was not in place. In addition, given the ferocity of the surge and storm waves that struck long sections along this alignment; it is not clear that a relatively thin veneer of compacted clay would have been sufficient to help very much.

As shown in the map of Figure 6.1, this levee frontage is one of only two locations where the levees protecting the three main protected basins of New Orleans are exposed directly to storm waves crossing a large body of Gulf waters (Lake Borgne) without the protection of significant swamp grounds on their outboard sides. The swamp grounds (and cypress trees) serve to damp the energy of the storm waves, reducing their height and velocity, and thus their erosive potential. It was unfortunate that this section that was so exposed to severe (unprotected) storm waves was also not yet up to full design grade, and that large portions were comprised of highly erodeable sand and lightweight shell sand fill.

It should be noted that the only other section of levee protecting one of the three main basins of New Orleans that was also exposed to open water storm waves (without significant outboard side swamp and cypress protection) is the "sister" section to the north; at the southeast corner of the New Orleans East protected basin (facing south, fronting Lake Borgne.) As discussed in Chapter 7, that "sister" section was also constructed using dredge spoils from the excavation of an adjacent shipping channel (the GIWW channel in that case), and was also comprised largely of highly erodeable sands and shell sands. That section, too, eroded catastrophically and represented the largest source of the floodwaters that catastrophically flooded the New Orleans East protected basin.

The exact nature of the erosion and breaching that occurred along this frontage section has not yet been fully agreed upon by the various investigation teams. It is the view of our

investigation that sections of this levee frontage appear to have eroded and begun to be breached prior to the storm surge reaching its full height (of approximately +16 to +19 feet, MSL) by as early as about 5:30 to 6:00 a.m.

Figure 6.10 shows the calculated hydrograph developed by IPET at this location, showing storm surge rise vs. time at this location as estimated by IPET (IPET, Second Interim Report, April 2006.) "Storm surge" is the mean water level between storm waves and troughs, so the additional height of waves, plus "run-up" as waves arrive at the levees must be added to determine when and to what extent the waters overtopped the levees. This is further complicated by the significant variations in crest elevation along this not yet completed levee frontage. The analytical prediction of Figure 6.10 matches well with the similar numerical hydrodynamic modeling performed by Team Louisiana (Kemp and Mashriqui, 2006), and both models are fairly well calibrated against regional observations of water elevations at numerous locations. The two investigation teams (IPET and Team Louisiana) differ significantly, however, in their calculated wave heights and frequencies along this MRGO frontage. IPET have calculated longer period storm waves typical of more "open ocean" conditions, and Team Louisiana have calculated shorter period waves constrained by lack of depth within the Lake Borgne embayment.

Figure 6.11 shows a schematic illustration of two different sets of erosion mechanisms for the levees along this frontage. Figure 6.11(a) shows simple "sheet flow" overtopping. This is a common mode of concern for many river levees, and also for many earth dams. In this mode, as the water flows over the top and then flows like a sheet down the rear-side slope of the levee embankment, the velocity of flow down the rear slope face accelerates and the shear stresses (erosive forces) induced by the flow increase with this increased velocity. Accordingly, erosion is initially most pronounced low on the back slope face (where the flow velocities become highest), and the embankment is eroded from the back side until the crest is breached (whereupon rapid flow through the crest rapidly enlarges the original breach.) This is the mechanism that is the customary principal design focus for the flood control levees in this region; excepting the large rivers such as the Mississippi River where scour produced by longitudinal flow of the river current itself is also a major concern.

Figure 6.11(b) illustrates two additional potential sets of erosion modes likely to have been active along sections of the MRGO frontage levees. One is the attacking of the outboard side (water side) face of the levee by storm waves. These high energy waves can scallop and erode the outboard face. They can also rush up the face toward the crest, and can erode "notches" in the crest from the front side. Subsequent waves can then pass through these notches, especially as the storm surge continues to rise, and the flow can widen the notches and also erode the back face levee slope (as discussed above as "sheet flow overtopping erosion".) This exploitation and widening of crest notches is called crenellation, after the crenellation (notched shape) that often tops castle walls.

Figure 6.11(b) also illustrates seepage flow passing through the embankment section, and then eroding soil as it exits through the lower portion of the back side slope face. This "through flow" can cause significant erosion if the embankment soils are pervious, as was the case along significant portions of the MRGO frontage levees. As this type of erosion occurs primarily in the lower back slope face region that is also most prone to erosion by sheetflow

overtopping, it can be difficult to separate field evidence of these two types of erosion as to cause.

The highly erodeable (and pervious) sands and shell sands that comprised significant sections of the levees along this frontage were vulnerable to all three types of erosion, and would have been expected to have been damaged by waves and by through flow from the rising storm surge well before the storm surge actually overtopped some sections. Evidence of front face scalloping erosion, and "notching" at the crest and front crest lip of levees along this MRGO frontage section are presented in Figures 6.12 and 6.13.

Methods and procedures for calculation of rates of likely erosion due to the various erosive mechanisms likely to have been operating along the critical MRGO levee frontage are not well-established, and there is little agreement within the profession as to how the erodeability of the various materials present (fill types, and fill placement and compaction states.) A number of members of the ILIT team made their own estimates of likely rates of erosion, based on their perceptions of the likely fractional content of various fill types, and the types of erodeability data presented and discussed in Chapters 9 and 10, and in Appendix I. These estimates also required judgmental assessment of through flow potential, wave runup magnitudes and velocities, numbers of wave cycles at different times (and thus different storm surge stage levels), etc.

The resulting estimates varied considerably, but all agreed that there was a high likelihood that initial breaching would have initiated well before the storm surge approached within several feet of the low points along the crests along this critical levee frontage. This appears to correlate well with the observation that massive amounts of storm surge flows filled and then pushed across the open swamplands behind the MRGO frontage levees, and then crossed over the secondary (Forty Arpent) levee and filled the populous zones to the south to elevations as high as +12 feet above mean sea level.

This is further supported by the observed behavior of the "sister" levee frontage section at the southeast edge of the New Orleans East protected basin. This section, which was also comprised in part of highly erodeable fill materials dredged from the adjacent shipping channel excavation (in that case the GIWW channel), and which also fronted Lake Borgne directly, without significant outboard side swamps or cypress to dam and suppress wave energies, was clearly breached and admitted large volumes of floodwaters well before the storm surge approached the levee crests. Timing along this "sister" section, and crest heights and storm surge heights, are better documented (see Chapter 7, Section 7.3.2) than along the MRGO frontage section, as the resultant New Orleans East flooding was definitively noted and captured on videotape by workers at the nearby Entergy power plant.

As shown in Figure 6.1, it was intended that the levees along this outer frontage would bear the brunt of the storm surge. Any overtopping flow, or even flow through localized breaches, would then have available a wide swath of undeveloped swamp land into which it could flow and pond. At the back side of this swampland a lower secondary levee (the Forty Arpent Levee) was then situated to protect the populous areas to the south. Unfortunately, the unexpectedly rapid and catastrophic erosion of this outer frontage levee allowed the storm

surge to flow virtually unimpeded across the open swampland before the storm surge had begun to subside significantly.

The Forty Arpent levee was only a "secondary" levee, with crest heights on the order of Elev. + 7.5 to + 10 feet (MSL), and it was not intended to have to face the full brunt of a largely undiminished rising storm surge. As a result, the storm surge passed easily over this secondary levee, and pushed rapidly into the populated areas of St. Bernard Parish, as described previously in Chapter 2. As is arrived rapidly, and prior to significant abatement of the storm surge, the floodwaters ponded to an unexpectedly high elevation of approximately +12 feet above mean sea level. Homes and businesses on "high ground" (at elevations several feet and more above sea level) were thus unexpectedly flooded, and the depth of flooding in lower-lying areas was especially severe. The massive inrushing floodwaters also had large lateral force, and pushed homes aside from their foundations (as shown previously in Figure 2.19), tossed cars like toys (see Figure 6.15), deposited large fishing boats in residential neighborhoods (Figure 6.16), and left large branches of trees on the roofs of numerous homes (e.g.: Figure 6.17).

Interestingly, the smaller (secondary) Forty Arpent levee was severely overtopped along much of its length, but it suffered relatively little erosional damage as a result. This appears to be because it was constructed of significantly better materials than the outer (MRGO frontage) levees; the Forty Arpent levee appears to have been constructed primarily of clay, with good intrinsic resistance to erosion. Figure 6.14 shows a section of the Forty Arpent levee that was apparently significantly overtopped, but which suffered only slight "cosmetic" erosional damage as a result.

The use of highly erodeable sand and shell sand fill was unfortunate along the exposed MRGO frontage levee section, and the consequences were severe. Damage to the populated areas of St. Bernard Parish was catastrophic, and the floodwaters from this populous area next began to make their way westwards towards what was now the already doomed Lower Ninth Ward.

6.3 The Two large Breaches on the East Bank of the IHNC at the Lower Ninth Ward

As the storm surge from Lake Borgne pushed westward along the east-west trending channel of the GIWW/MRGO that separates the St. Bernard and New Orleans East protected basins, it raised the water levels in the IHNC and produced two massive breaches on the east bank of the IHNC (at the western edge of the Lower Ninth Ward). These two breaches occurred at approximately 7:30 to 7:45 a.m., at an IHNC water level of approximately Elev. + 14 to +14.5 feet (MSL), as shown in Figure 6.18 (which shows a hydrograph of measured water levels vs. time in the IHNC channel.)

6.3.1 The IHNC East Bank (South) Breach at the Lower Ninth Ward

The larger of these two breaches was the south breach, and this is shown in Figure 6.19 (which is a repeat of Figure 2.13). This was a very long breach, nearly 900 feet in length, and the inrushing waters entered the adjacent community with great force. As shown

in Figure 6.17, homes for several blocks were ripped from their foundations and scattered, usually in splinters, eastward across the inboard neighborhood.

Figure 6.19 also shows the sheetpile curtain that had supported the floodwall at the crest of the earthen levee at this section. It is interesting to note that the sheetpiles (which were cold-rolled steel sections) remained interlocked throughout the cataclysmic failure and the ensuing hydrodynamic loading of the massive inrushing floodwaters. The concrete floodwall is largely absent from the tops of these sheetpiles, as the sheetpiles have been stretched out (like an accordion), flattening their bent flanges in order to accommodate the extension imposed on them by the inrushing flow.

Figure 6.19 also shows a large steel barge that passed inward through this section, and came to rest near the southern end of the breach. This raised the question as to which came first; the barge or the breach?

Figure 6.20 shows the large barge, in its final resting position (prior to being cut apart with torches to remove it) atop a small yellow bus. This was not the initial resting location of this barge immediately after hurricane Katrina, however. Initially, after Katrina, the barge had come to rest a bit farther to the east. It was then re-floated several weeks later when the temporary breach repair failed during the second hurricane surge produced by hurricane Rita on September 24, 2005 (see Chapter 11), and came to rest at its current position at that time. The small yellow school bus also arrived between hurricanes Katrina and Rita, having been appropriated and used for interim transport and then abandoned in its location as shown.

There is a single large dent low on the side of the barge just around the left side of the bow (not quite visible in Figure 6.20), and a pronounced scrape on the bottom of the barge at that same location. Most of the concrete floodwall was failed in extension and flexure, with its reinforcing steel (rebar) fairly extended. There was one single section of wall which clearly evinced a major impact, however, and that was at the extreme southern end of the breach. Figure 6.21 shows a close-up view of the floodwall at this location. The rebar is compressed and bent, and the concrete crushed at this location. It was the consensus view of our investigation team that the barge had scraped along the wall and then impacted the end of the wall at this location.

As this was the extreme southern end of the very long breach; this impact was not the cause of the breach and failure. Instead, the barge was apparently traveling southwards along the IHNC (driven by the prevailing storm winds at that time) and was drawn into the breach by the inflowing waters. The barge did not enter cleanly into the breach, but struck at the south end before passing in.

That does not mean that the barge might not have struck the floodwall twice (or more times) before finally impacting the southern end of the breach, but our investigation's view is that there are other modes of failure that would have been expected to fail this section without any need for help from the barge, so that the likelihood is that the barge slipped its moorings and was eventually drawn in through a breach that was already well developed.

Figure 6.22 shows the trench that was eroded by water that passed over the top of the concrete floodwall at the south end of the large breach. (The barge can be seen at the right in this photo.) Overtopping and scour occurred at both ends of this breach feature, and the resulting scoured trenches reached depths of up to 5.5 feet in sections that did not subsequently fail. It is, of course, not possible to determine whether deeper scouring/trenching might have occurred at the actual breach inception location, as the embankment and foundation soils at the center of the breach were deeply scoured out by the massive flows in through the breach. One of the potential failure modes evaluated by our (ILIT) studies was the possibility that this scour had sufficiently laterally unbraced the concrete floodwall (and its supporting sheetpile curtain) that the lateral force of the elevated canal water was able to displace it laterals and foment a resulting breach.

Figure 6.23 shows our ILIT re-interpretation of the original boring data along this section of the east bank of the IHNC, with the locations of the two large breaches indicated. The boring data was far too sparse along this section for the importance of the design (the inboard population and properties being protected) and for the complexity of the local geology. In addition, widely spaced borings along the approximate levee centerline do not provide an adequate basis for development of appropriate cross-sections for analysis and design. An effort was made to perform pairs of borings (one roughly at the crest and another at the inboard toe) at selected locations so that cross-sections could at least be attempted, but this was still an inadequately sparse investigation. The foundation investigation for the design of these levees and floodwalls was inadequate for a project of this scope and importance, and the minor savings in drilling, sampling and testing are now dwarfed by the massive costs of the failures that resulted; both property damages and loss of life.

Figure 6.24 shows the cross-section used for our analyses of this south breach. The two pre-Katrina ("initial design") borings, Borings B-4 and B-4T, were supplemented by three additional CPT probes performed by the IPET investigation (IHBR-6.05C, 5.05C and 16.05C), and two additional borings and a CPTU probe that were performed by our ILIT investigation (Borings IHNC-S-BOR-1 and CON-1, and CPTU IHNC-S-CPT-1). The cross-section of Figure 6.24 shows the tragic failure to extend the sheetpile curtain to sufficient depth as to cut off underseepage flow through the laterally pervious "marsh" deposits at this site.

The upper embankment fill is a moderately compacted imported clay, which is underlain by an older "fat clay" (CH) fill apparently comprised of locally available lacustrine clays. The upper foundation soils are then dominated by thick deposits of high plasticity clays (CH), punctuated by two layers of marsh deposits, and there is a relatively thin but continuous stratum of low plasticity silt (ML) underlying the lower marsh unit.

Subsequent to the completion of the levee embankment and floodwall, additional sandy fill was placed on the outboard (water) side of the levee to raise the ground surface slightly above mean canal water level. Some buildings and facilities had been constructed on this made ground, but these had been removed prior to hurricane Katrina.

Figure 6.25 shows plots of data regarding strength properties vs. depth for the soils from the silt layer down (from Elevations -19 to -50 feet, MSL) beneath (a) the levee crest,

and (b) at the inboard toe of the levee (under far lesser embankment overburden). The detailed procedures and relationships used to process the CPTU data, and then to overlay the additional UUTX data to develop these plots, are presented and discussed in detail in Chapter 8, and this will not be repeated here. The lower unit of lacustrine clay clearly shows two overconsolidation "crusts" as a result of surface desiccation during early "stands" in the accretion of these deposits, and they are more normally consolidated at greater depth. These clays, in the end, do not appear to have participated in the failure that occurred.

Similarly, the relatively thin silt stratum (ML) also shows evidence of overconsolidation, and this gives it sufficient strength that it too is uninvolved the failure.

Figure 6.26 shows similar plots regarding strength properties of the far more critical upper foundation soil strata between elevations of approximately +0 to -20 feet (MSL). These deposits, consisting of interlayered marsh and clay units, are the critical soils at this site.

As described in detail in Chapter 8, a number of different approaches were taken to the processing of the available field and laboratory test data in order to evaluate and characterize these soils. Based on the CPTU measurements within the marsh deposits (both at this site, and at the 17th Street canal breach site) values of B_q were developed, and then based on the relationships of Lunne et al. (1994) and Karlsrud et al. (1996), a value of N_{kt} = 15 was selected for transposing the CPTU tip resistance values to the estimates of undrained shear strength that are plotted in Figure 6.26. The resulting values were then converted to values of Su/P as shown in the far right figure of Figure 6.26, and these appear to infer three desiccation-induced overconsolidation profiles corresponding to surface exposure at three times during the evolution of these deposits. The relationship of Mayne and Mitchell (1988) was then used, again as described in Chapter 8, to cross-check the resulting relationship between Su/P vs. OCR as a function of Plasticity Index (PI, %) for these deposits using the available UUTX laboratory test data. These were found to be consistent. Finally, the limited available in situ vane shear test data, and the UUTX laboratory test data, was co-plotted with the CPTU-based strengths, and these too were judged to be consistent (with allowances for sample disturbance and vane insertion disturbance in these soils of variable fibrous organic content).

Similar processing resulted in selection of a value of N_{kt} = 15 for processing of the CPTU data for the silty clay (CH/CL) stratum lying between the two "marsh" deposits. This differs from the value of N_{kt} = 12 that was used to process the CPTU data for the deeper layer of gray lacustrine clay of high plasticity, and it reflects the lower plasticity of this upper clay unit. Once again, the limited available in situ vane shear test data and UUTX laboratory test data were then co-plotted with the strengths as interpreted by the CPTU, and were found to be consistent (as shown).

Figure 6.27 shows the geometry and principal input parameters used to model and analyze this section using the finite element analysis program PLAXIS (2004). The "soft soil" constitutive model within PLAXIS was used to model all of the uppermost soil strata, so that both undrained and partially drained conditions could be studied within an effective stress framework. Shear strengths from Figures 6.25 and 6.26 were reduced by 15% in the marsh strata, and by 20% in the clay strata, to account for differences between the field (in situ) test

conditions and the laboratory test conditions, and the direct simple shear (DSS) conditions expected to dominate the critical field performance behavior in these analyses.

Initial analyses were performed to model the incremental construction of the levee embankments in order to establish the initial stress conditions for the subsequent analyses of the overall section performance and stability during hurricane Katrina's storm surge loading. Figure 6.28 shows the deformed mesh at the end of staged construction and consolidation under the levee embankment loads. Overconsolidation stress profiles beneath the crest, and beneath the inboard levee toe, well matched those from the available field data, and the consolidation properties were iterated slightly until the final (post-consolidation) settled profile matched well with the observed field configuration.

Analyses were then performed in which the water level within the canal was progressively raised. Transmission of pore pressures beneath the wall (and beneath the sheetpiles) was very rapid, and nearly "steady state" pore pressure conditions developed very rapidly beneath the inboard side of the levee after each increase in water levels as the lateral transmissivity of the marsh deposits was high, and the system was initially well saturated. The rate of water level rise (and subsequent decline) in the canal was based on the hydrograph of Figure 6.18.

Figure 6.30 shows conditions calculated just as the canal water level reached the top of the concrete floodwall. Plotted in this figure (as color contours) are levels of relative shear strain (shear strain developed, divided by shear strain to failure) within the levee embankment and foundation soils. As shown clearly in this figure, two distinct failure mechanisms are beginning to develop. The lower one is a shear surface concentrated at the interface between the base of the upper gray clay (CH/CL) layer and the underlying layer of marsh deposits, and the upper failure surface attempting to develop is concentrated at the interface between the top of the upper marsh stratum and the lower levee embankment fill section. Both of these mechanisms represent the results of underseepage-induced increases in pore pressures being "trapped" at the bases of less pervious overlying strata. These pore pressure increases are decreasing the strength and stiffness of the soils at these two critical interfaces.

At the water stage shown in Figure 6.30, a gap has begun to form at the outboard side of the floodwall and its supporting sheetpile curtain. When effective tensile stress was calculated between the floodwall/sheetpile wall and the adjacent soils, the analysis was temporarily stopped, the tension was eliminated by changing the mesh details to insert a small gap (and to insert hydrostatic water pressures within the gap), and the analysis was resumed. This was done iteratively, as water levels continued to rise, so that the progressive development of a water-filled gap between the floodwall/sheetpile curtain and the outboard section of the levee embankment could be modeled. At this section, within reasonable parameter variations modeled, gap formation generally initiated at canal water levels on the order of Elev. +11.5 to +13 feet (MSL), and the gap then tended to progress fairly rapidly to the base of the sheetpiles (within the next 1 to 2 feet of water level rise in the canal).

Figure 6.31 shows calculated conditions for a canal water level at Elev. +14 feet (MSL). At this stage, water is now overtopping the floodwall, the gap at the outboard side of the sheetpile wall is developed to full depth, and stability failure is occurring on the

uppermost of the two potential failure surfaces. This upper failure is serving to "protect" against further development of the lower failure surface (which can also be seen in this figure.) If the upper failure surface is strengthened a bit, to prevent the upper failure, then the lower failure becomes critical.

Figure 6.32 shows the postulated path to failure based on the finite element (PLAXIS) analyses performed. In this figure, the Factor of Safety at any given surge height was assessed by stopping the analysis at each stage of water level rise, and evaluating Factor of Safety by means of progressive c – Ø reduction. Two sets of conditions were analyzed; conditions in which a "gap" was allowed to form on the outboard side of the sheetpile/floodwall (and the gap was allowed to fill with water as it opened), and a second set of analyses without allowing the opening of this gap. The light blue diamonds in Figure 6.32 represent conditions without gapping, and the yellow circles represent conditions with progressive opening of a water-filled gap.

As shown in this figure, the gap begins to open as the storm surge rises near to the top of the floodwall (at a surge elevation of about +11 to +12 feet, MSL), and the increasing lateral push of the rising surge waters finally destabilizes the system at a surge elevation of approximately +12 to +13 feet, MSL. This appears to agree closely with the observed field timing and surge levels at failure.

These analyses also include the "excavation" of a trench at the levee crest at the rear side of the floodwall representing the results of overtopping erosion at the north and south ends of the breach. The depth of this eroded trench was taken as rapidly increasing from none to 5 feet in depth as overtopping began to pass over the top of the floodwall. Additional analyses were performed for eroded trench depths of up to 7.5 feet, but this did not significantly affect the overall results; simple erosion of a scoured trench behind the floodwall, even as deep as 7.5 feet, was not sufficient as to cause the observed failure and breaching of this levee/floodwall section. The scoured trench behind the floodwall did contribute a bit to the enhancement of lateral displacement (and resultant water-filled gapping) on the outboard side, but it does not appear to have been the principal factor at this failure and breach site.

Additional analyses were performed to further evaluate both the seepage flow vs. time, and the overall stability of this levee and floodwall section. Seepage analyses, as well as conventional Limit Equilibrium analyses (by several methods, but these agreed closely and results presented herein are for Spencer's Method) were performed using the program package GEO-SLOPE/W.

Figures 6.33 and 6.34 show the cross-sections and meshes used for conventional limit equilibrium and coupled seepage analyses of this same breach section. As shown in Figure 6.35, the rapid lateral flow through the main marsh stratum distorts the flownet, carrying pressures and equipotential contours along as it passes beneath the embankment. Figure 6.36 shows a close-up view of calculated pore pressure contours for a storm surge elevation of +14 feet (MSL). Over a considerable area at and inboard of the levee toe the net pore pressure uplift forces are slightly greater then the weight of the relatively light soils present, representing conditions prone to potential "uplift" or "blowout" at this critical location.

Figure 6.37 shows a close-up view of hydraulic gradients at this same canal surge stage. As expected, the exit gradients calculated at the toe are slightly unstable with regard to initiation of seepage erosion and piping for the relatively lightweight soils present.

A key question in these analyses is the rate at which rises in outboard side canal water levels manifest themselves in the form of increased pore pressures beneath the inboard side of the levee embankment. That, in turn, is largely a function of the lateral permeability modeled within the marsh strata, and assumptions regarding degree of initial saturation.

It was our investigation team's observation that lateral permeability was very high within at least some of the sub-strata of these variable marsh deposits, both at the two east bank IHNC breach sites at the edge of the Lower Ninth Ward, as well as at sites along the drainage canals at the north end of the main (downtown) New Orleans protected basin. Hydraulic response at nearby boreholes was very rapid, and evidence of the occurrence of high water pressures and underseepage was noted at several locations. Investigators from the IPET team were surprised by difficulties in dewatering a very shallow excavation to recover large block samples of peaty "marsh" deposits at the 17th Street canal breach site for subsequent centrifuge testing. In addition, persistent reports of underseepage and ponding of waters along this IHNC frontage at the west edge of the Lower Ninth Ward, and contractor's significant problems with dewatering of excavations along this same frontage, all bespoke of high lateral permeability within these strata.

The values of lateral permeability used in these analyses were based on experience with similar geologic units from other regions, our own field observations, and the accumulated reports indicating high lateral permeability. A best-estimated coefficient of lateral permeability of $k_h \approx 10^{-2}$ cm/sec was modeled for the most open of the marsh sub-strata, and parametric sensitivity analyses were performed for values of k_h that were five times higher, and values that were an order of magnitude (factor of 10) lower.

Figures 6.38 and 6.39 show results of these sensitivity analyses. Transient flow analyses were performed in which canal water levels were raised progressively, beginning with assumed fully equilibrated ("steady state") conditions with a canal water elevation of about +5 feet (MSL) at ~11:00 p.m. on the night of August 28th (after many hours of relatively slow surge rise to that level), then rising progressively to elevation +9 feet (MSL) by about 3:30 a.m. on the morning of August 29th, and then rising a bit more rapidly to elevation +14.4 feet (MSL) by about 8:30 a.m. (It should be noted that the failure and breach occurred at about 7:45 a.m., but that these transient flow analyses were carried forward to at least 9:00 a.m. to more fully examine progressive flow and pore pressure development.)

Figure 6.38 shows calculated pore pressures vs. time at location 1, at the top of the lower marsh stratum, directly below arrow "D" near the inboard toe of Figures 6.35 through 6.37. The horizontal light blue line at the top of this figure represents the "steady state" conditions that would eventually develop for a canal water level rise to Elevation +14.4 feet (MSL) if infinite time were allowed for full equilibration and development of steady state flow. The lower diamonds represent calculated transient pore pressures at Location 1 for the best-estimated lateral permeability of the marsh deposits, and for the upper and lower bound permeabilities. As shown in this figure, the variation in permeability does not exert a major

influence on the pore pressures, given the relatively slow rate of canal water level rise, and pore pressures within the main marsh deposit at the base of the inboard levee toe are on the order of about 85% to 92% of full "steady state" pressures at the apparent time of failure (at about 7:45 a.m.)

Figure 6.39 shows similar transient flow analyses to calculate pore pressure development at various depths beneath the location of arrow "D" in Figures 6.35 through 6.37, using the best-estimated permeabilities. Again, pore pressure development is fairly rapid, and lags only moderately behind outboard side canal water level rise.

Figure 6.40 shows the calculated gradients at the top of the lower marsh stratum (the blue line) at about 7:45 a.m., based on best-estimated permeabilites, and the exit gradients at this time as well (the red line.) The toe exit gradients are marginally unstable, given the lightweight materials present, and represent conditions likely to give rise to the inception of piping erosion.

Figure 6.41 shows the progressive development of pore pressures at the top of the lower marsh stratum vs. time. As shown, there is a considerable area over which the hydraulic uplift forces progressively grow to become somewhat larger than the total overburden stresses; representing a condition that could lead to uplift and "blowout" at this location.

Finally, Figures 6.42 and 6.43 shows analyses of limit equilibrium (Spencer's Method) for failure surfaces passing (a) along the interface at the top of the upper marsh stratum, and (b) along the interface at the top of the (lower) main marsh stratum, for a canal water elevation of +14 feet (MSL). Both sections are marginally unstable at this condition with regard to lateral translation of the inboard portion of the levee embankment, pushed sideways by the outboard side canal water pressures (including a water-filled gap at the outboard side of the sheetpiles), and in both cases the foundation soil strengths have been critically reduced by underseepage-induced pore pressure increases.

Figures 6.42 and 6.43 likely overestimate the overall lateral translational stability at this stage of canal water level rise, as it is likely that piping erosion would have at least initiated at the inboard toe region by this stage, and the calculated hydraulic uplift pressures in the inboard toe region are high enough that "buckling" of the passive toe block helping to restrain the lateral translations of Figures 6.42 and 6.43 might further reduce the overall stability.

As shown by these analyses, as the canal water level rises above about + 13 to +14 feet (MSL) this section becomes analytically unstable by a number of potential mechanisms, all of them associated with underseepage flow passing beneath the sheetpile curtain. These potential mechanisms are:

1. Seepage erosion and piping due to excessive exit gradients at the inboard toe.

2. Hydraulic uplift or "blowout" at the inboard toe.

3. Translational stability failure, as a result of reduction in strength of the foundation soils at the inboard side due to underseepage-induced pore pressure increases.

Based on the length of the breach feature (approximately 900 feet), it is most likely that the mechanism that won the race to failure at this site was translational instability due to underseepage-induced pore pressure increases, and resulting strength reduction within the inboard side foundation soils. It is certainly possible, however, that all three mechanisms contributed at least in part. Figure 6.44 shows the postulated most likely path to failure, based on both the finite element and the coupled transient flow/limit equilibrium analyses. The postulated failure path proceeds up the "un-gapped" limit equilibrium path at the right of Figure 6.44 until a gap on the outboard side of the sheetpiles begins to open and fill with water at a canal water elevation of about +12 to +13 feet (MSL). The failure mechanism then transitions to the "water-filled gap" limit equilibrium case (the left-most line in Figure 6.44), and as the canal water level continues to rise the overall section becomes unstable (in underseepage-induced lateral translational foundation instability) at a canal water level of approximately +14 feet (MSL).

This contradicts the initial conclusions of the Draft Final Report by the IPET investigation (IPET; June 1, 2006), and also the initial hypotheses of the ASCE and NSF-sponsored field investigation teams; all of which favored the hypothesis that the failure and breach at this site had resulted from overtopping flow over the floodwall which eroded a trench along the back side of the wall (as shown previously in Figure 6.22), resulting in laterally unbracing the wall so that it was then pushed over by the surge water pressures on its outboard side.

Our investigation's view is that, while overtopping and trenching were in fact occurring, it was underseepage-induced instability that actually developed the more critical mechanism that led to failure at this site.

The depth of overtopping-induced trench erosion at the north and south shoulders of the breach never reached depths greater than 4.5 to 5 feet. It might be inferred that a low spot along the crest of the floodwall occurred at the breach location, and that somewhat deeper erosional trenching resulted, but our finite element analyses show that even excavation of a trench as deep as 7 to 8 feet by overtopping erosion does not sufficiently unbrace the wall as to foment a lateral wall failure at surge heights overtopping the wall by as much as 1.5 feet. Instead, the contribution of overtopping and erosion of a trench at the inboard toe of the floodwall was more likely to have, at best, slightly accelerated the timing of this failure by adding to the propensity of the floodwall to deflect laterally slightly and thus develop a "gap" into which water could flow and then apply additional lateral pressure against the sheetpile curtain to promote the lateral translational stability of the inboard side of the levee embankment.

Our finite element analyses, performed with eroded "trenches" of various depths (from none, to as much as 8 feet) suggest that the trench erosion likely helped to exacerbate the initiation of "gapping" at the outboard side of the floodwall at a slightly lower canal water elevation than would have occurred without this erosion, but that it was not the critical contributor to this failure.

This is an important issue with regard to repair and reconstruction. The USACE has expended considerable effort and resources to replace "I-walls" with "T-walls", and to install concrete splash pads behind additional I-wall sections, in order to prevent failures due to the mechanism of overtopping, erosion of a trench at the rear side of the I-walls, and failure due to the resulting unbracing of the wall sections. Although also useful, this will not also deal effectively with the underseepage issues that appear to have been the actual cause of failure at this site; and there appear to be unreasonably short sheetpile curtains (insufficient as to effectively cut off underseepage flows) at other locations throughout the New Orleans regional flood defense system. This is a potentially pervasive problem throughout the system, and it should be evaluated system-wide, and remedied as necessary.

The IPET Final Draft Report notes that possible modes of failure initially considered at this site included "sliding instability and piping and erosion from underseepage." The report then goes on to say

> *Piping erosion from underseepage is unlikely because the I-walls were founded in a clay levee fill, a marsh layer made up of organics, clay and silt, and a clay layer. Because of the thickness, the low permeabilities of these materials, and the relatively short duration of the storm, this failure mode was considered not likely and was eliminated as a possible mode of failure.*

This greatly underestimates the permeability, and especially the laterally permeability of the marsh deposits. It also continues the very dangerous assumption that underseepage was not a serious problem for "short duration" storm surge loading that plagued the original design of many sections of the New Orleans regional flood defense system, and led to use of sheetpile curtains that were far too short to effectively (and safely) cut off underseepage flows. At least four major failures (and breaches) that caused large portions of the overall flooding damage and loss of life during hurricane Katrina appear to have been principally due to lack of appreciation of underseepage, and resulting inadequate (short) sheetpile cut-offs. These are the major breach at the west bank near the north end of the London Avenue drainage canal (see Section 8.3.9), the major breach at the east bank of the London Avenue drainage canal farther to the south (see Section 8.3.8), and the two breaches on the east bank of the IHNC at the west end of the Lower Ninth Ward discussed in this current section and in Section 6.3.2. Exoneration, a priori, of underseepage dangers should be discontinued immediately, and underseepage analyses should be required for the full regional flood protection system.

Demonstration that underseepage occurred at this site can be based on arguments of analogous conditions and levee performance at this site, and at the London Avenue drainage canal breach sites, as well as at the site immediately to the north (as described in the next section.) It can also be based on the observed difficulties encountered by McElwee Construction in dewatering an excavation near the breach site immediately to the north (due to massive underseepage flow through the marsh deposits that were not adequately cut off at that site either.)

In addition, as noted in the IPET Draft Final Report in discussion of the two massive breaches at the west end of the Lower Ninth Ward:

Although it is clear that the walls were overtopped, and that their stability was compromised by the erosion that occurred, it is also clear that one of the east side breaches occurred before the wall was overtopped. Eyewitness reports indicate that the water level in the 9th ward near Florida Avenue was rising as early as 5:00 AM, when the water level in the IHNC was still below the top of the floodwall. Stability analyses indicate that foundation instability would occur before overtopping at the north breach on the east side of the IHNC. This breach location is thus the likely source of the early flooding in the 9th Ward. Stability analyses indicate that the other three breach locations would not have failed before they were overtopped.

Unfortunately, even IPET's own analyses do not suggest a high likelihood of failure of the north breach section at the canal water levels present as early as 5:00 a.m. (approximately Elev. + 9 feet, MSL), so this would not appear to be the explanation for the observed water in the neighborhood. Instead, it is proposed that the observed water rise on the inboard (protected) side near Florida Avenue was more likely the result of large underseepage flows through the highly pervious "marsh" deposits along this frontage.

Finally, clear and uncompromising evidence of the high lateral permeability of these deposits **at this site** is presented in Figure 6.45, which shows a well-developed classic crevasse splay that resulted from reverse underseepage through these same highly pervious marsh deposits as the ponded floodwaters drained out from the Lower Ninth Ward after the hurricane passed.

The New Orleans District of the USACE must stop "assuming" that short-term storm surges do not pose a significant risk associated with underseepage, and should instead begin assuming that such underseepage is a potential risk and that it must be addressed either: (1) with testing and analyses, (2) by means of sheetpile curtains extended deeply enough to effectively cut off potentially dangerous underseepage, or (3) by means of wider and heavier levee embankments (including inboard side stability berms) and the use of filtered drains at the inboard toe of the levee to "vent" and thus draw down the potentially dangerous pore pressures in that vicinity.

6.3.2 The IHNC East Bank (North) Breach at the Lower Ninth Ward

Figure 6.46 shows an aerial view of the partially repaired breach that occurred just to the north of the breach discussed in the preceding Section 6.3.1. This second breach feature was a much shorter feature, with a length of only approximately 250 feet.

This narrower, deep failure had similar initial geometry and stratigraphy to that of the far longer section immediately to its south, as shown by the cross-section in Figure 6.47. At this section, there is only the one main marsh layer, but most of the other soil conditions are very similar to those at the adjacent breach section to the south.

Figures 6.47 and 6.48 show the cross-section and finite element mesh used for limit equilibrium and coupled seepage analyses of this section.

Soils data at this site were sparse, and consisted of a single pre-Katrina boring (located nearby but just off-site, and with higher embankment overburden loads than at the breach site), two ILIT borings and one ILIT CPTU probe, and several additional IPET CPT probes. We were never able to fully determine the locations of the IPET CPT's in plan view, but it was assumed that they were located in adequate proximity as to be "representative", and their elevations were known with good precision so that these data could be used to at least cross-check the other data available. Cross-checking the limited data (mainly from two CPTU probes) with the data from the breach site immediately to the south showed strong compatibility; accordingly similar properties (and OCR profiles, etc.) were modeled for similar soil units at this section.

Figure 6.49 shows the calculated flownet equipotential lines for a canal water surge elevation of +14 feet (MSL). Once again, as with the larger breach just to the south, the flow travels through the continuous marsh layer that was left frustratingly open to flow by the shallow sheetpiles that were an inadequate cut-off at this site.

Figure 6.50 shows pore pressure contours for the same conditions as Figure 6.49. Once again the hydraulic uplift pressures represent potential instability with regard to lifting or "blowout" of the thin surficial strata of impervious and relatively lightweight soils overlying the marsh stratum at and near the inboard toe.

Similarly, as shown in Figure 6.51, seepage exit gradients at and near the inboard toe are massively unsafe with regard to the initiation of seepage erosion and piping in these relatively lightweight soils.

And finally, as with the adjacent breach section to the south, the section is also marginally unstable with regard to limit equilibrium (Spencer's method), as shown in Figure 6.52, as a result of underseepage-induced pore pressures and resultant loss of strength. The most critical failure surface this time passes through (and largely within) the main marsh layer, though a secondary failure surface concentrated near the interface between this marsh layer and the overlying clay layer has a nearly similar (unstable) factor of safety.

Figures 6.53 and 6.54 show calculated transient pore pressures (6.53) at the top of the marsh stratum beneath the inboard toe of the levee, and (6.54) at various depths beneath the inboard levee toe. As for the breach section immediately to the south, the upper and lower bound lateral permeability estimates are also shown in Figure 6.53; and again a large fraction of the overall rise in canal water levels has resulted in corollary water pressure increases at the inboard toe region by about 7:00 to 8:00 a.m.

Figure 6.55 shows the progressive increase in pore pressure at the top of the marsh stratum vs. time, and the pore pressures are high enough to pose a very high risk of hydraulic uplift (or "blowout") at the inboard toe region.

Figure 6.56 shows a potential path to failure by means of lateral translational foundation instability; reaching a condition of marginal lateral instability (with full

development of a water-filled gap at the outboard side of the sheetpile curtain) at a canal water elevation of approximately +13 to +14 feet (MSL).

Here again, as with the larger breach section immediately to the south, this breach section is analytically unstable by a number of potential mechanisms, all of them associated with underseepage flow passing beneath the sheetpile curtain. These potential mechanisms are:

1. Seepage erosion and piping due to excessive exit gradients at the inboard toe.

2. Hydraulic uplift or "blowout" at the inboard toe.

3. Translational stability failure, as a result of reduction in strength of the foundation soils at the inboard side due to underseepage-induced pore pressure increases.

As with the larger breach to the south, it is our investigation's position that despite the fact that overtopping (and resultant erosion at the inboard toe of the floodwall) was also occurring, this failure was the result of one or more of the underseepage-induced mechanisms above. (Two or more of these may have acted in concert.)

This site has a well-documented history of underseepage problems; McElwee Construction had great difficulty dewatering an excavation at this site during earlier construction, and residents of the neighborhood had also previously reported problems with seepage at the inboard toe.

Based on the geometry of the post-failure configuration (see Figure 6.46), this narrow, deep failure appears to have most likely caused by either by seepage erosion and piping, or by a combination of hydraulic uplift ("blowout") followed by piping. The calculated high exit gradients, and the hydraulic uplift pressures at the inboard toe region, would strongly support this.

The IPET interim draft report also concluded that foundation instability was the cause of the failure and breach at this site. The failure mechanism favored in those analyses, however, was based on a semi-rotational failure dominated by undrained shear failure through the soft clays underlying the marsh stratum, as shown in Figure 6.58. IPET concluded that this failure occurred at a relatively early stage, at a canal water level of only Elevation +9 feet (MSL), and that this early failure accounted for observations of ponding of water along this general levee frontage well in advance of the failure of the larger breach section to the south.

Figure 6.59 shows the IPET interpretation of shear strength data for this section, and the red lines are the IPET shear strength profiles for stability analyses (IPET: June 1, 2006.) In this figure, the values of undrained shear strength based on the CPT tip resistance data are based on a CPT tip factor of $N_k = 15$. This appears to be an overly conservative value of N_k within the lower clay stratum, as the CPT-based shear strengths within this stratum are significantly lower then the trend based on the unconsolidated-undrained triaxial tests on "undisturbed" samples obtained with a 5-inch diameter thin-walled fixed-piston sampler. In

any case, the shear strength profile used by the IPET analyses within this layer is well to the left (lower than) the vast majority of the data available.

Our own studies determined (based on B_q values from the CPTU) indicated that values of N_{kt} = 12 were more appropriate for this lower soft clay (CH) layer, and the resulting re-interpretation of this CPT data based on N_{kt} = 12 is shown (with a dark blue trace) super-posed over the previous Figure 6.59 in Figure 6.60. Similarly, the dark blue lines in Figure 6.60 show our (ILIT) interpretation of the layering at this location, and the light blue dashed lines show our interpretations of shear strength vs. depth at this section. The IPET shear strength interpretation, in addition to being low, was also based on the assumption that this lower clay stratum was normally consolidated over its full depth. As shown previously in Figures 6.25 and 6.26, our own interpretations showed several clear desiccation-induced overconsolidation profiles near the middle and top of this clay layer, and additional moderate overconsolidation near the base (likely to the base being well-drained and thus partially overconsolidated due to secondary compression), and these are reflected in our ILIT shear strength profile. In this figure, the CPTU-based shear strengths (based on N_{kt} = 12) can be seen to be in better agreement with the other shear strength data, and the overall shear strength vs. depth profile is more consistent with this data.

Repetition of the limit equilibrium analysis (Spencer's Method) of the failure surface shown in Figure 6.58, but using our own (ILIT) interpretation of undrained shear strengths within the critical lower clay layer (Figure 6.60) results in a calculated factor of safety, even conservatively assuming the presence of a water-filled gap on the outboard side of the sheetpile curtain, of FS = 1.89. This underestimates the actual overall Factor of Safety, which should actually be on the order of 10% to 15% higher based on three-dimensional considerations for this narrow, deep failure. It is therefore not likely that a deep, semi-rotational failure occurred, early on and at a relatively low canal water level, at this site.

The need of the IPET analyses to provide an early failure at this north breach site in order to explain the significant observed ponding of waters along this frontage prior to the occurrence of the large breach farther to the south, and to do so without consideration of underseepage as a potential source of this water, resulted in an apparently unrealistic analysis and an indefensible failure mechanism.

If the IPET team had been made aware of the pervasive history of underseepage problems along this frontage, they would surely have considered and analyzed underseepage-related failure modes for the two large breaches along this section of the east bank of the IHNC. This information was apparently not available to the IPET analysis team, however, reflecting insufficient communication between groups and teams across the overly modular, sub-team-organized IPET studies. In addition, the pervasive failure of the New Orleans District of the USACE to adequately consider and analyze underseepage during pre-Katrina design of considerable portions of the regional flood protection system was continued in the post-event IPET studies of these two failed sections.

The New Orleans regional flood protection systems need to be thoroughly re-assessed, and re-analyzed as necessary, with regard to potential additional underseepage-related

vulnerabilities. And then these must be mitigated in order to develop a safe and reliable overall system..

6.3.3 Summary

The two large breaches on the east bank of the IHNC (at the west end of the Lower Ninth Ward) both occurred at sites where overtopping occurred. Despite the occurrence of overtopping, and resultant erosion of trenches at the inboard sides of the concrete floodwalls, this overtopping does not appear to have been the cause of the two failures. Instead, these two failures appear to have resulted from underseepage-induced instability; either due to erosion and piping at the inboard toe, "blowout", or translational instability due to strength reduction in the inboard side foundation soils due to underseepage-induced pore pressure increases.

This represents a potentially critical difference from the findings to date from the Corps' IPET study; as the remedy for overtopping, trench erosion, and unbracing at the top of the floodwalls is very different from the remedy for underseepage-induced instability problems. The USACE has invested large resources to replace "I-walls" with "T-walls", and to install concrete splash pads behind additional "I-wall" sections. This is laudible, but it will not also effectively mitigate underseepage-related problems.

Remedies for the underseepage related problems revealed by these analyses would include either extension of the sheetpile curtains to greater depths in order to more effectively "cut off" underseepage, or widening of the levee embankments to the inboard side and installation of filtered drains at the inboard toes in order to safely draw down the underseepage-induced high pore pressures in that area.

Analyses of the IHNC failure sections, and of sections of the three drainage canals in the main (downtown) New Orleans protected basin (see Chapter 8), have shown that unreasonably short sheetpile curtains of too limited penetration as to effectively cut off underseepage are likely to be endemic throughout many parts of the New Orleans regional flood protection system. Indeed, the USACE at a number of breach repair sites is replacing sheetpiles with (pre-Katrina) lengths of 18 to 24 feet with far longer (deeper penetrating) sheetpiles with lengths of 60 feet and greater as part of the repair operations; an unusually frank admission that significantly deeper sheetpiles were warranted at those sections.

There is now a need to review, and to re-analyze as necessary, essentially the entire regional flood protection system with regard to potential vulnerability associated with underseepage (and inadequately deep sheetpiles), and to remedy these problems at sites where necessary in order to ensure overall safety of the system.

6.4 Summary and Findings

The catastrophic flooding of the St. Bernard and Lower Ninth ward protected basin was primarily due to: (1) catastrophic erosion of the MRGO frontage levees, and (2) a pair of large failures (and breaches) on the east bank of the IHNC at the west end of the Lower Ninth Ward.

The catastrophic erosion of large portions of the nearly 11-mile long MRGO frontage levees was the result in large part of the use of unsuitable sand and shell sand fills (with low resistance to erosion) for major portions of these embankments. Large portions of these fill materials came from spoils dredged from the excavation of the adjacent MRGO channel, and the short-term savings achieved by the use of these soils now pale in comparison to the massive damages and loss of life that resulted. Because these levees eroded so rapidly, and so massively, the storm surge was able to push largely undiminished across a wide area of undeveloped swampland behind the main frontage levees, cross a lower secondary levee (the Forty Arpent levee) that has not been intended to have to face an undiminished rising storm surge, and then charged into the populated zones of St. Bernard Parish with catastrophic consequences.

Because it passed so quickly and so completely through the frontage levees, the surge filled the St. Bernard basin to an elevation of +12 feet above sea level; inundating homes and businesses located well above sea level that had expected to be safe, and inundating lower lying properties to great depths.

The use of intrinsically highly erodeable fills, especially clean sands, and the even more dangerous lightweight shell sands, should be reconsidered. The use of such materials as levee embankment fill, especially without taking appropriate measures to mitigate the erosional hazards associated with these (e.g.: sheetpile cutoff, erosion protection and armoring of exposed slope faces and crests, etc.) is inadvisable when constructing levees intended to protect large populations at risk.

The two large breaches at the east bank of the IHNC (at the west end of the Lower Ninth Ward) both appear to have resulted not from overtopping, but rather from underseepage beneath the inadequately deep sheetpile curtains at these two sections. Overall, four of the eight most significant failures (breaches) that occurred during hurricane Katrina (the eight breaches that caused the greatest damages and loss of life) appear to have been due to inadequate attention to underseepage during initial design, and resulting sheetpile curtains that were far too short as to suitably cut-off or minimize these underseepage flows (see also Sections 8.3.8 and 8.3.9). This appears to be a widespread problem throughout the New Orleans regional flood protection system; the entire system should be re-evaluated with respect to this potential hazard, and mitigation implemented as necessary.

6.5 References

GEO-SLOPE/W (2004) “Complete Set of Manuals”, John Krahn (Edit.), Calgary, Alberta, Canada.

IPET – Interagency Performance Evaluation Task Force (2006) *Performance Evaluation Status and Interim Results*, Report 2 of a Series, Performance Evaluation of the New Orleans and Southeast Lousiana Hurricane Protection System, March 10, US Army Corps of Engineers.

Karlsrud,K., Lunne, T and Brattlien (1996) "Improved CPTU interpretations based on block samples", Nordic Geotechnical Conference, 12 Reykjavik 1996. Proc, Vol.1, pp 195-201.

Kemp, P., (2006), Personal Communication

Lunne, T., Lacasse, S., and Rad, N.S., (1994) "General report: SPT, CPT, PMT, and recent developments in in-situ testing", Proceedings, 12th International Conference on soil mechanics and foundation engineering, Vol.4, Rio de Janeiro, pp. 2339-2403

Mashriqui, H., (2006), Personal Communication

Mayne, P,W and Mitchell, J.K (1988) "Profiling of Overconsolidation Ratio in Clays by Field Vane", Canadian Geotechnical Journal, Vol 25, No 1, February, pp 150-157.

PLAXIS Finite Element Code for Soil and Rock Analyses (2004). "Complete Set of Manuals", V8.2 , Brinkgreve yVermeer (Edit.), Balkema, Rotterdam, Brookfield.

U.S. Army Corps of Engineers. (1968) *Lake Pontchartrain, LA and Vicinity Lake Pontchartrain Barrier Plan, Design Memorandum No 2, General Supplement No. 8, Inner Harbor Navigation Canal Remaining Levees,* New Orleans District, New Orleans LA.

U.S. Army Corps of Engineers. (1969) *Lake Pontchartrain, LA and Vicinity Lake Pontchartrain Barrier Plan, Design Memorandum No 2, General Supplement No. 8, West Levee Vicinity France Road and Florida Avenue,* New Orleans District, New Orleans LA.

U.S. Army Corps of Engineers. (1971) *Lake Pontchartrain, LA and Vicinity Lake Pontchartrain Barrier Plan, Design Memorandum No 2, General Supplement No. 8, Modification of Protective Alignment and Pertinent Design Information I.H.N.C. Remaining Levees West Levee Vicinity France Road and Florida Avenue Containerization Complex,* New Orleans District, New Orleans LA.

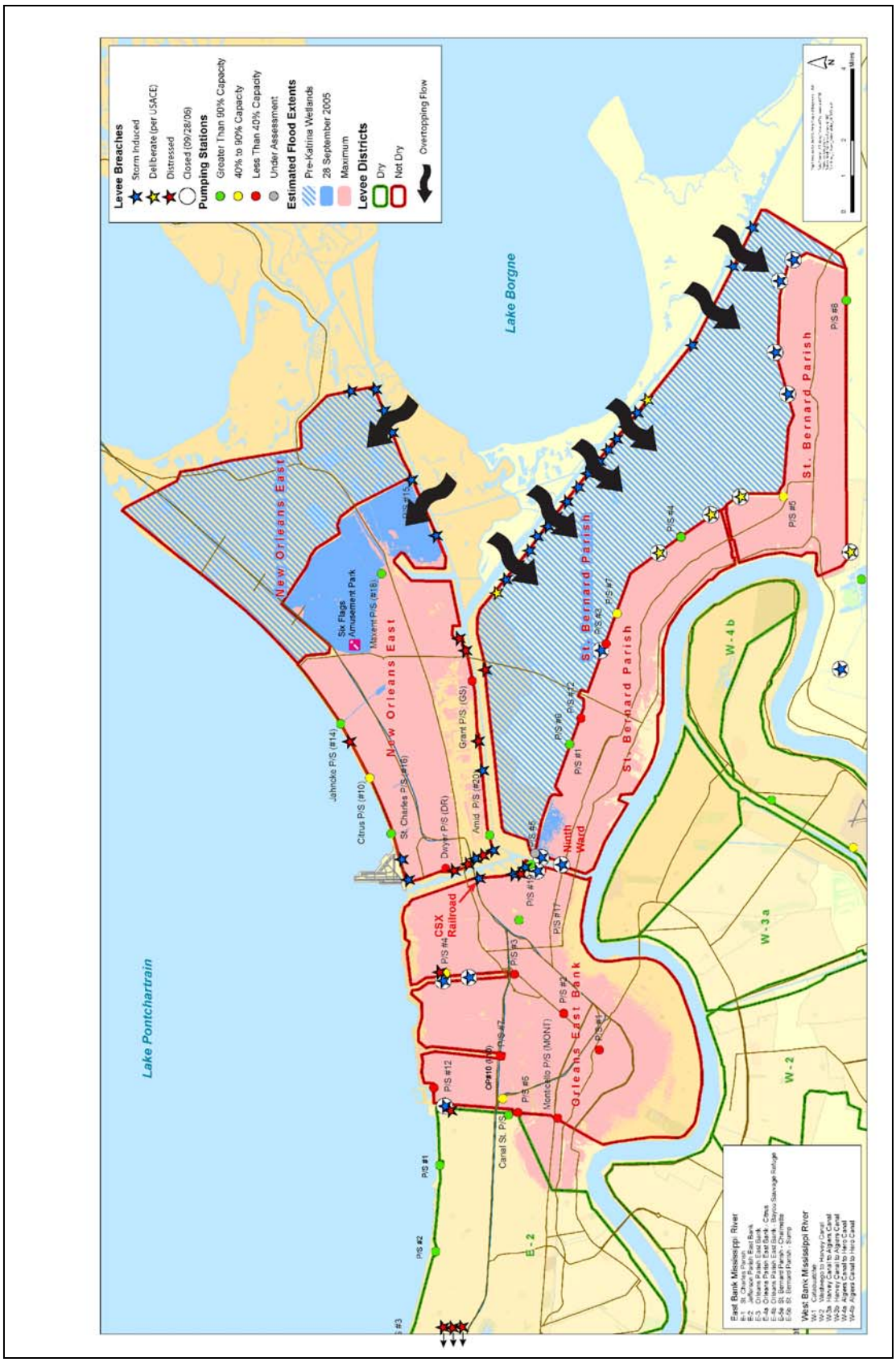

Figure 6.1: Map showing locations of levee breaches and distressed levee sections.

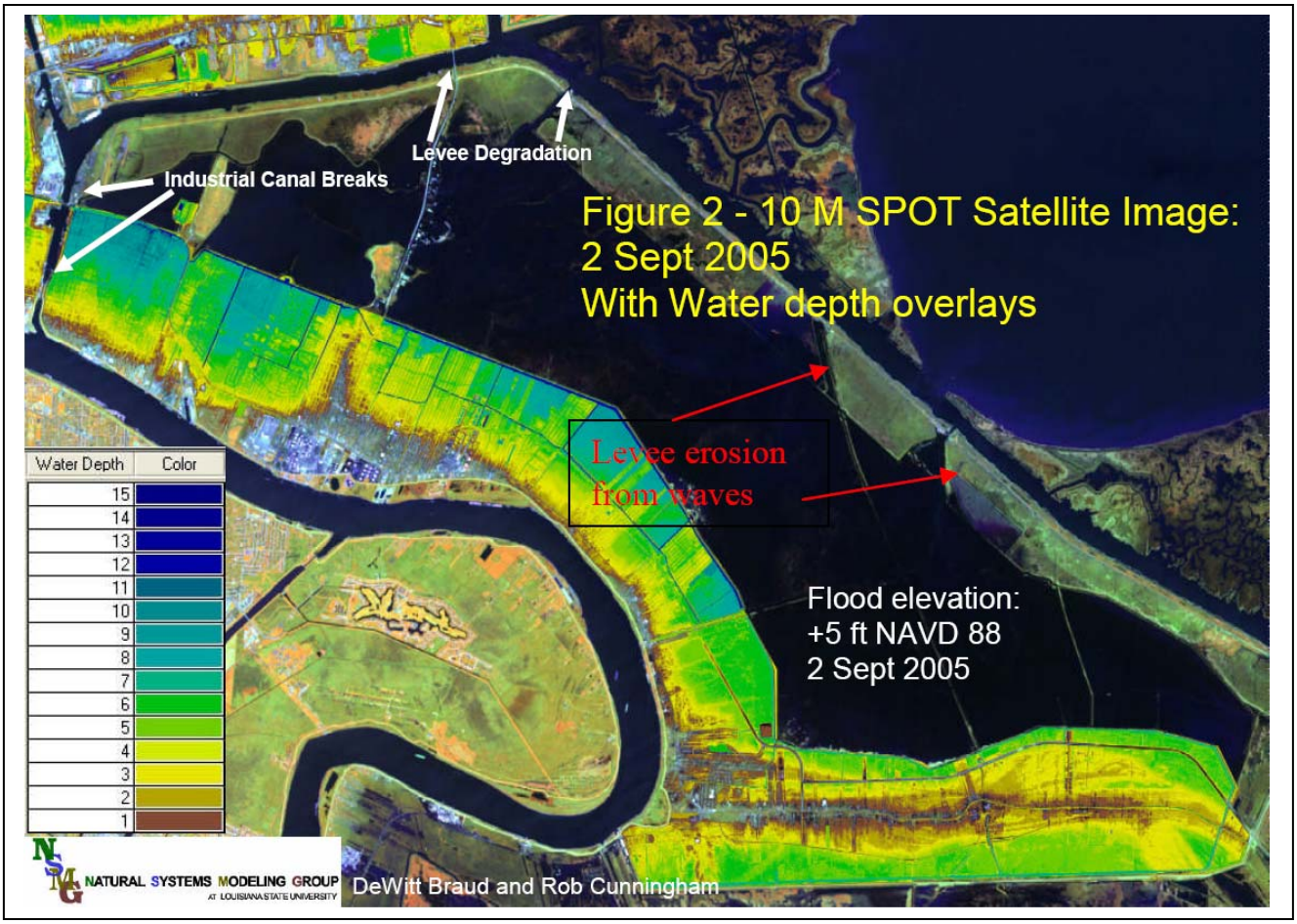

Source: LSU Hurricane Center

Figure 6.2: Depth of flooding of St. Bernard Parish and the Lower Ninth Ward on Sept. 2nd (4 days after Hurricane Katrina).

Figure 6.3: Catastrophically eroded levee section along the northeast frontage of the St. Bernard Parish protected basis, fronting the MRGO channel.

Figure 6.4: Catastrophic erosion of levee embankment leaving central sheetpile curtain; also along the northeast frontage of the St. Bernard Parish protected basin fronting the MRGO channel.

Figure 6.5: Extensive erosion of levees along the MRGO frontage at the northeast edge of the St. Bernard Parish protected area.

Figure 6.6: View of sheetpiles left behind at catastrophically eroded section of the MRGO frontage levee.

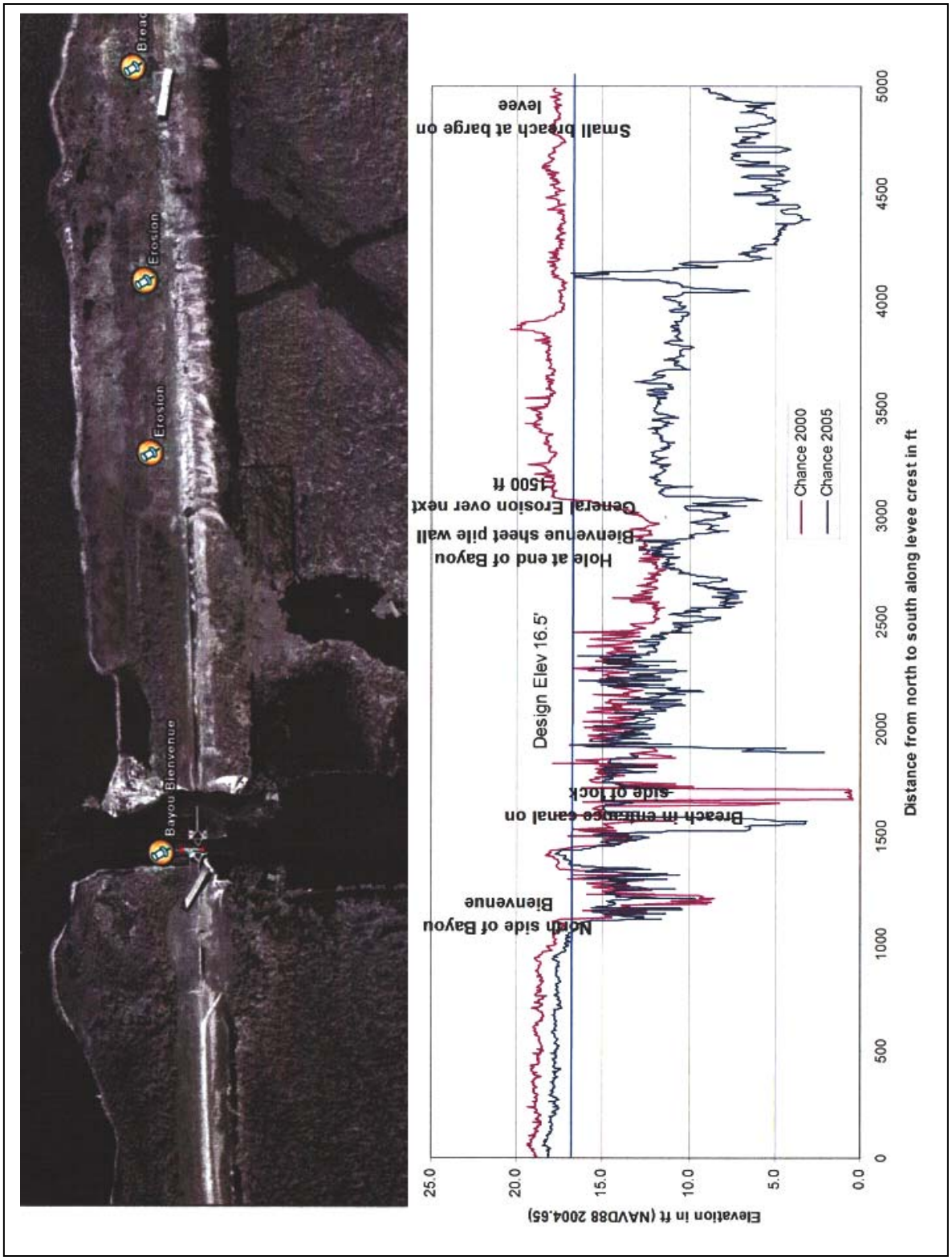

Figure 6.7: LIDAR survey data showing crest elevations before and after hurricane Katrina along a section of the MRGO frontage levees at bayou Bienvenue, and corresponding post-event plan view aerial photo along the same section.

Figure 6.8: Large eroded breach at the contact between the south end of the massive concrete navigational lock structure at Bayou Bienvenue and the adjacent levee section.

Figure 6.9(a): Aerial view of the large erosional breach at the contact between the north end of the concrete navigational lock structure and the adjoining levee embankment at Bayou Dupres.

Figure 6.9(b): View looking to the inboard side from the breach shown in Figure 6.5 above; showing eroded shell sand detritus deposited from the breach.

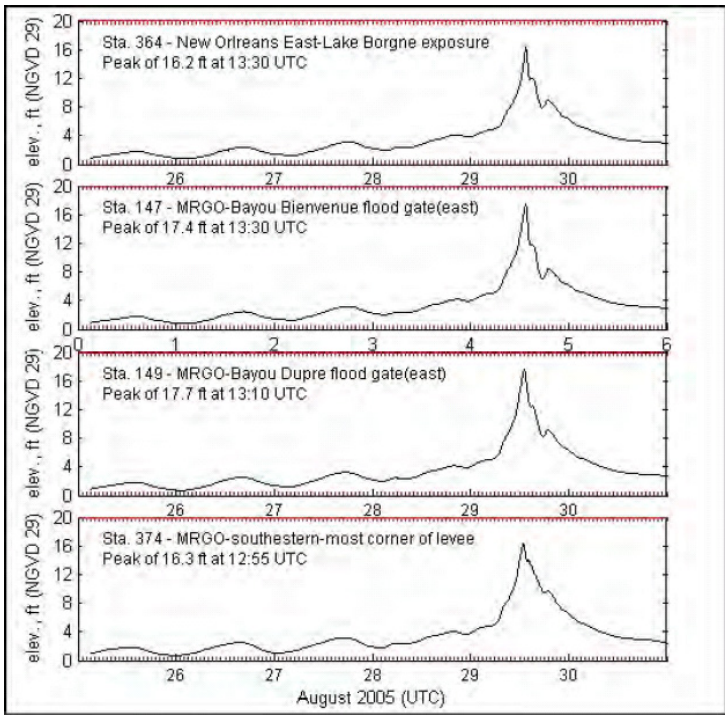

Figure 6.10: Approximate hydrograph of storm surge elevation (feet, MSL) vs. time at the west end of Lake Borgne. [IPET Interim Report, April, 2006]

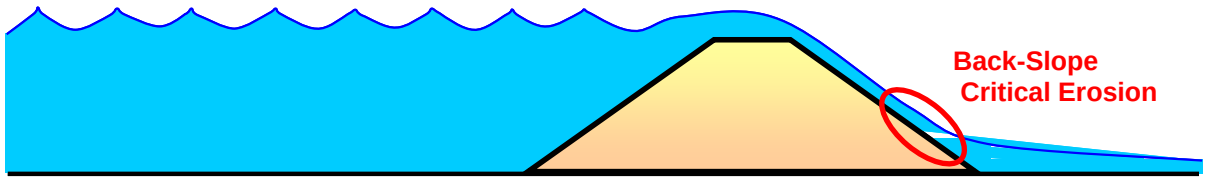

(a) Sheet flow overtopping erosion of the lower back slope face

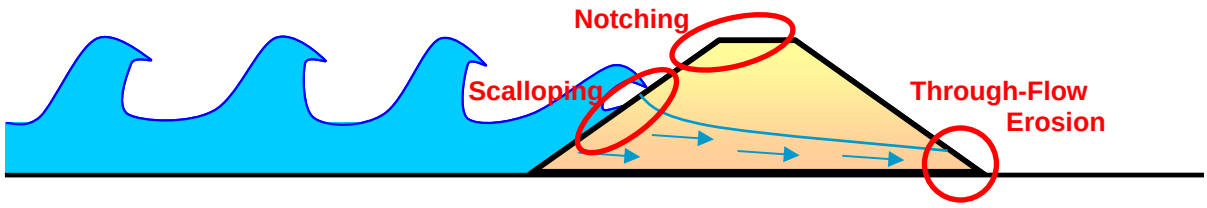

(b) Wave erosion of the front face, and through-flow erosion of the lower back face

Figure 6.11: Schematic illustration of two different sets of modes of levee erosion.

Figure 6.12: Photo of outboard side wave-induced erosion on the MRGO levee frontage at the northeast edge of the St. Bernard/Ninth Ward protected area.

Figure 6.13: Photo of outboard side levee erosion and crest "notching", as well as crenellation, due to storm wave erosion and overtopping along the MRGO frontage levees at the northeast edge of the St. Bernard/Ninth Ward protected area.

Figure 6.14: View of the secondary (Forty Arpent) levee across the middle of the St. Bernard protected basin.

Figure 6.15: View of tree limbs and detritus on roofs of homes in St. Bernard Parish.

Figure 6.16: Car tossed and flipped in St. Bernard Parish.

Figure 6.17: Boat deposited in neighborhood in St. Bernard Parish.

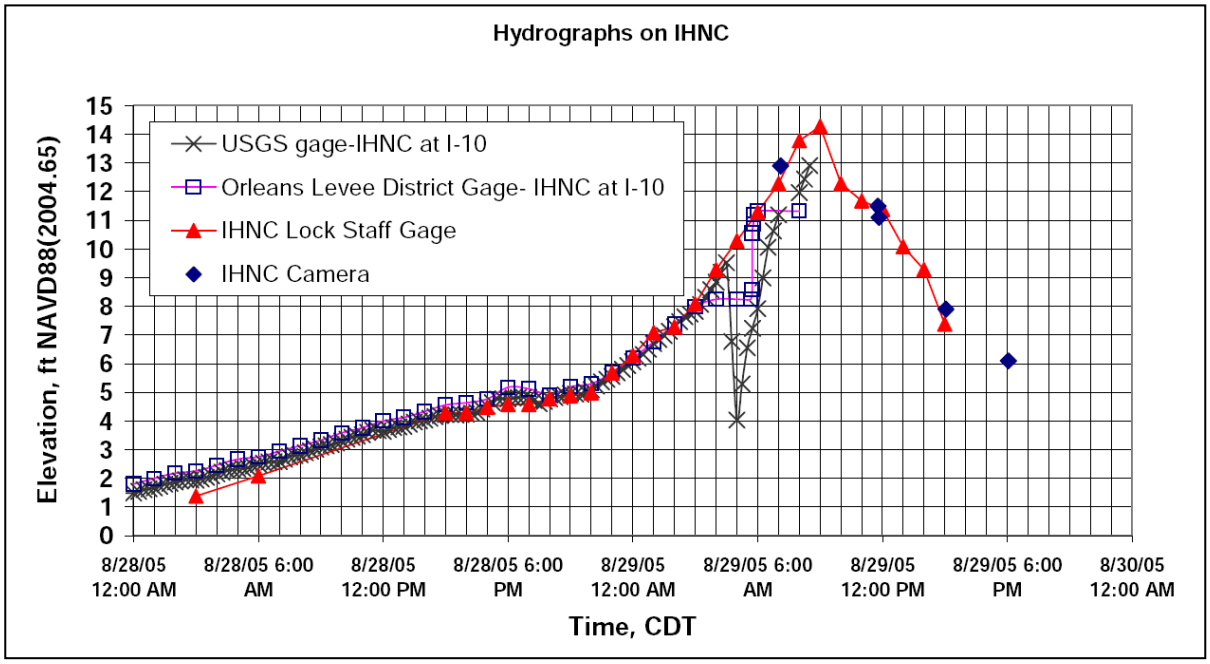

Source: IPET Interim Report No. 2; April, 2006

Figure 6.18: Hydrographs showing measured (and photographed) water levels at gage stations along the Inner Harbor Navigation Channel (IHNC).

Figure 6.19: Oblique view of the (south) levee break at the Inner Harbor Navigation Canal into the lower Ninth Ward.

Photograph by: Rune Storesund

Figure 6.20: Close-up view of the large barge that entered through the south breach at the east bank of the IHNC at the west end of the Lower Ninth Ward.

Photograph by: Rune Storesund

Figure 6.21: Close-up view of crushed (impacted) concrete floodwall at the south end of the south breach at the east bank of the IHNC at the west end of the Lower Ninth Ward.

Photograph by: Rune Storesund

Figure 6.22: Eroded trench at the rear (inboard) side of the floodwall at the south end of the south breach at the east bank of the IHNC at the west end of the Lower Ninth Ward.

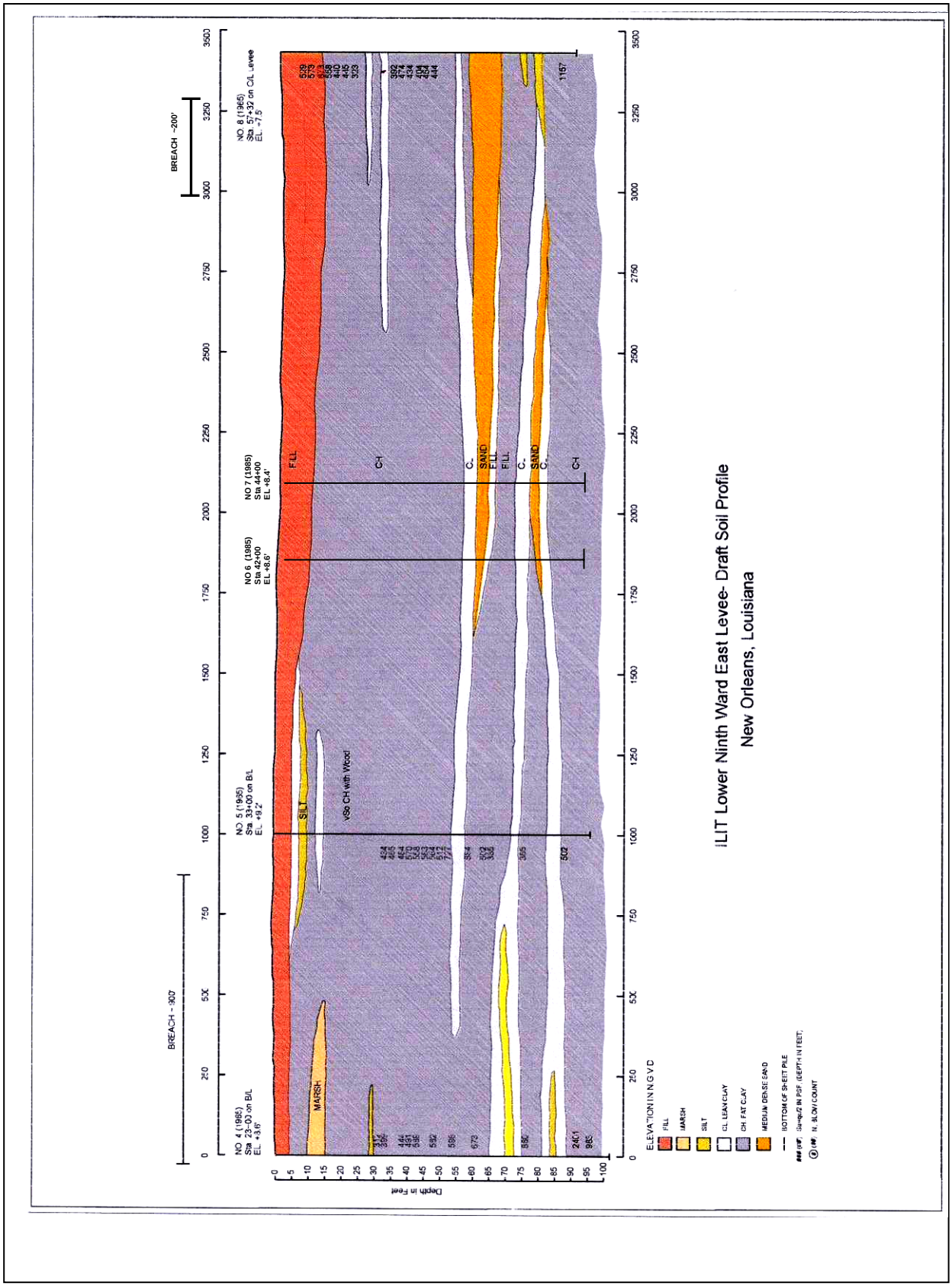

Figure 6.23: Re-interpreted longitudinal subsurface soil profile, showing location of breach section on the east bank of the Lower ninth Ward Levee.

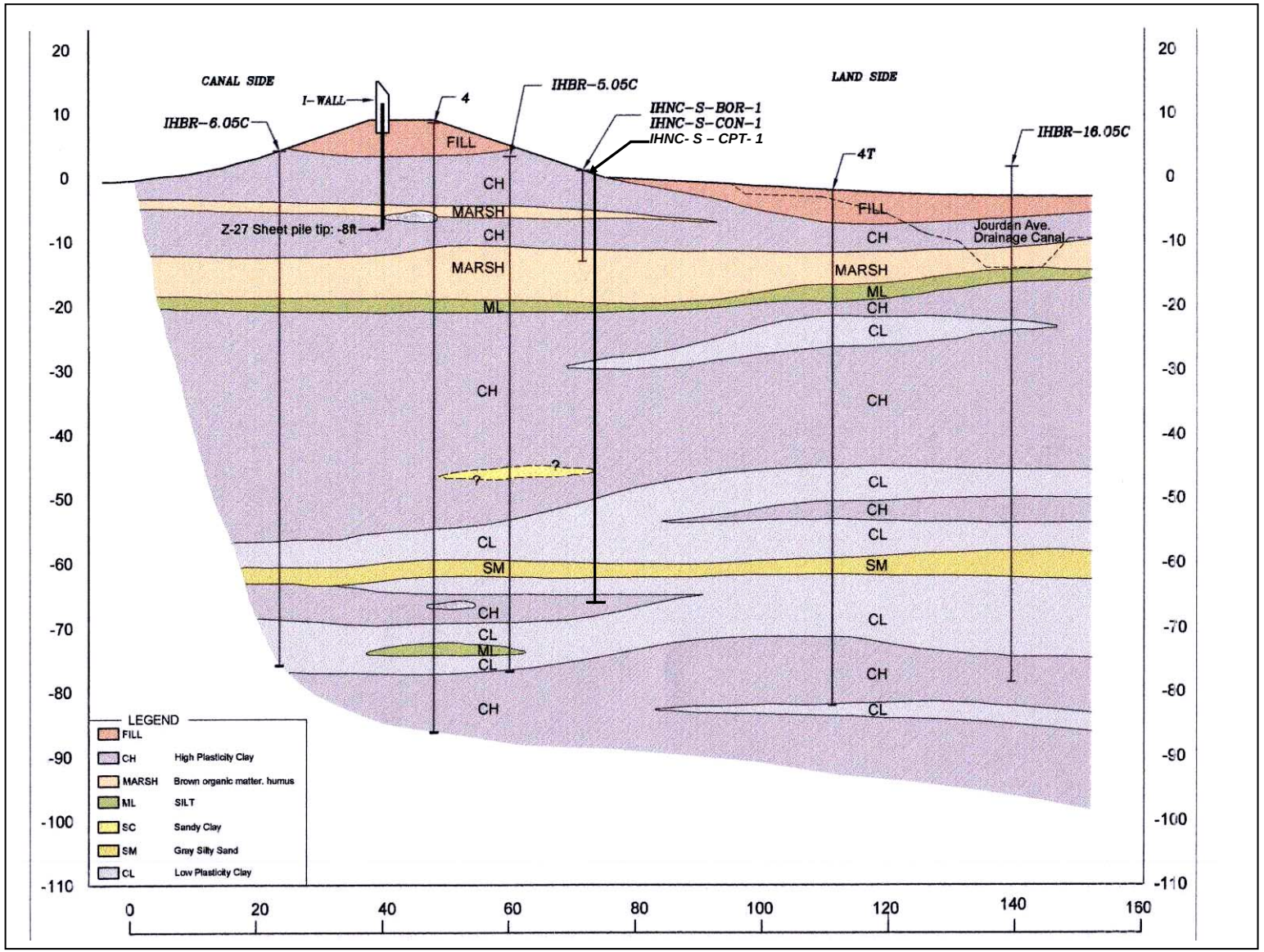

Figure 6.24: Cross-section showing location of borings for Lower Ninth Ward, East Bank, South Breach.

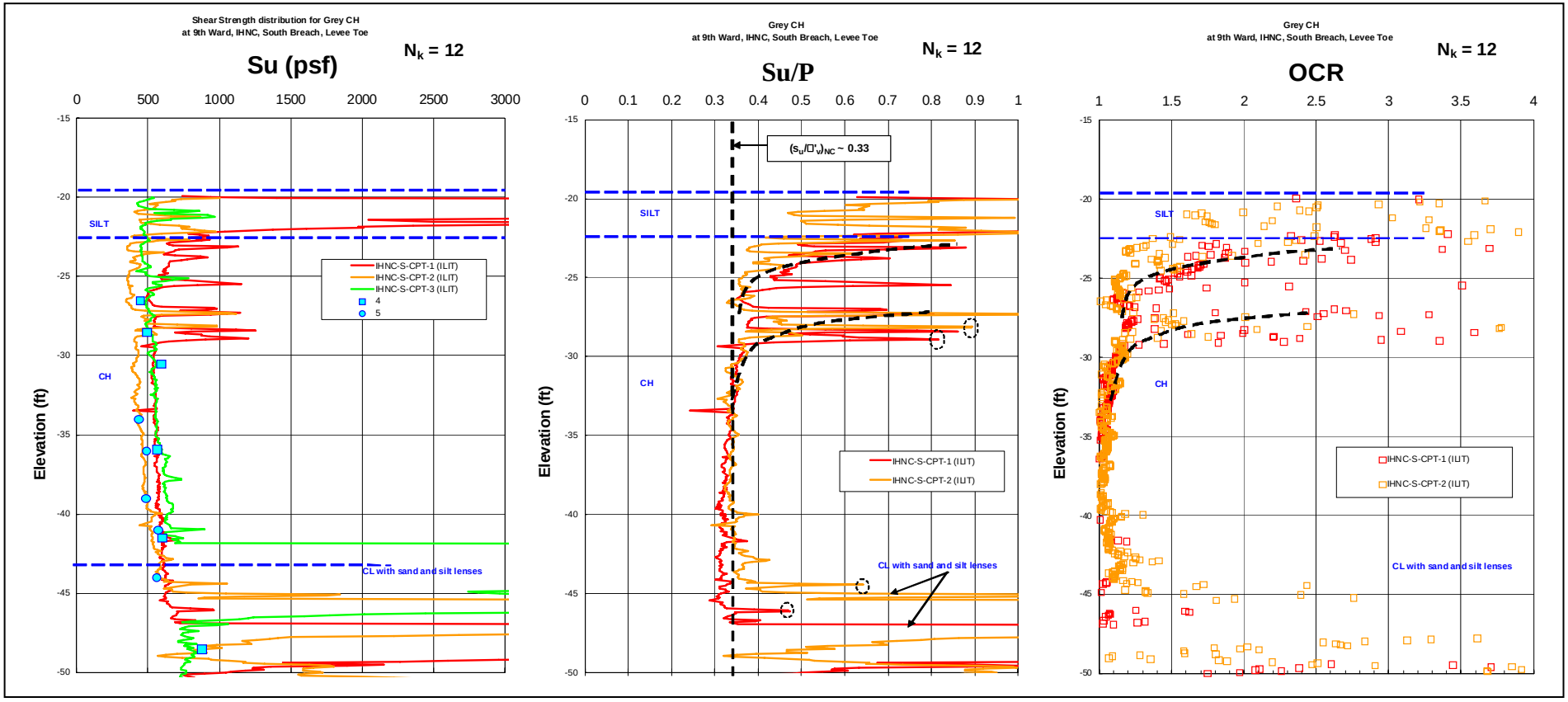

Figure 6.25: Plots of (a) OCR vs. Depth and (b) S_u vs. Depth for the soft gray marsh clay (CH) at the inboard toe and further to the landside (not under levee embankment overburden pressure) – Lower Ninth Ward, IHNC East Bank, South Breach site.

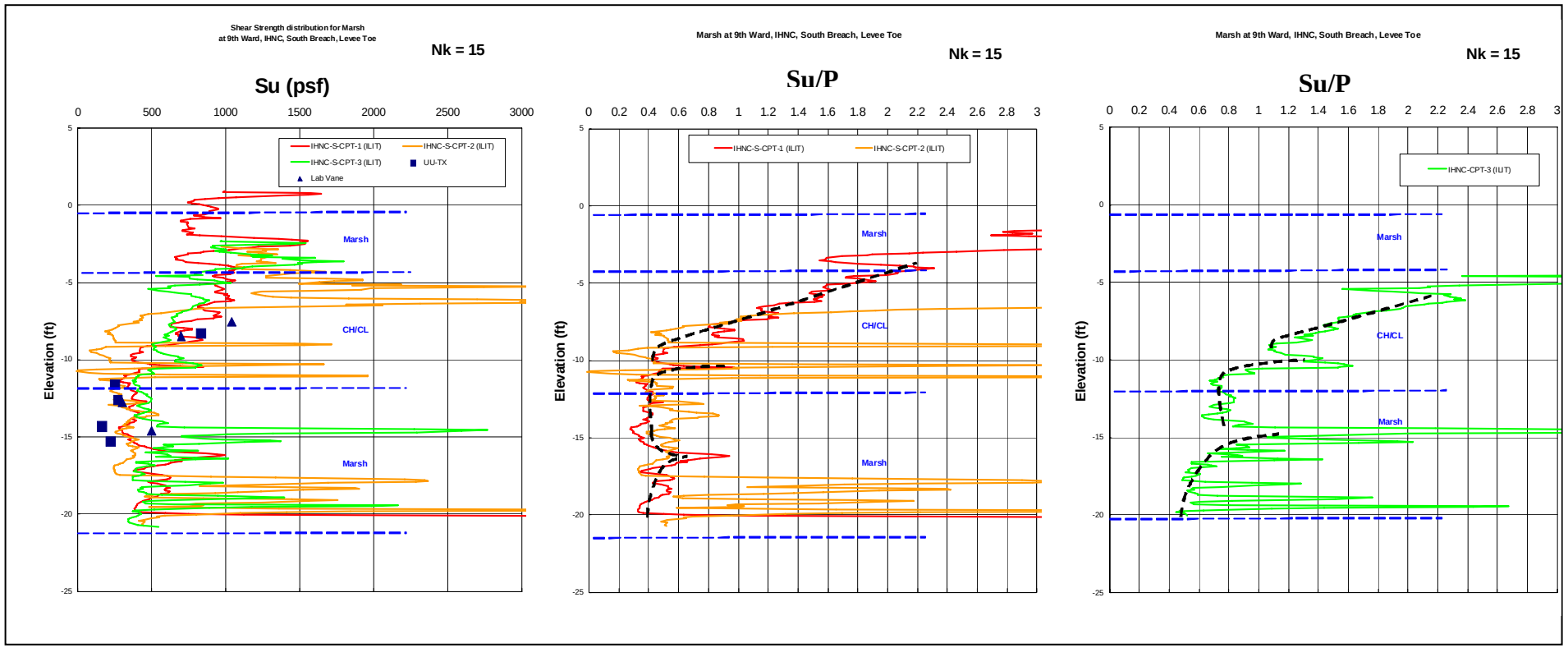

Figure 6.26: Plots of (a) OCR vs. Depth and (b) S_u vs. Depth for the shallow marsh and clay deposits at the inboard toe and further to the landside (not under levee embankment overburden pressure) – Lower Ninth Ward, IHNC East Bank, South Breach site.

ID	Soil Model	Name	Type	g_unsat [lb/ft^3]	g_sat [lb/ft^3]	k_x [ft/day]	k_y [ft/day]	nu [-]	E_ref [lb/ft^2]	c_ref [lb/ft^2]	phi [°]
CF Bottom	Mohr Coulomb	ML-silt (Compacted Fill)	Undrained	105	115	0.0028	0.00028	0.35	234000	900	0.001
		Gray Clay (bottom)	Undrained	90	90	0.0028	0.0028	0.3	155000	800	0.001

ID	Soil Model	Name	Type	g_unsat [lb/ft^3]	g_sat [lb/ft^3]	k_x [ft/day]	k_y [ft/day]	lambda* [-]	kappa* [-]	n_ur [-]	K0nc [-]	M [-]	c_ref [lb/ft^2]	phi @ pref [°]	OCR
M2	Soft Soil	Marsh 2	Undrained	80	80	28.3	2.8	0.21	0.033	0.15	0.60	1.90	0	36	1.1
M1		upper marsh	Undrained	80	80	28.3	2.8	0.2105	0.033	0.15	0.60	1.90	0.0001	36	2.25
ML		silt	Undrained	85	85	28.32	2.8	0.1	0.02	0.15	0.61	1.27	0.001	23	2
CH2		Gray Clay (CH)	Undrained	90	95	0.00028	0.000028	0.1684	0.03	0.15	0.63	1.24	0.0001	22	2.25-1.70
CH3		Gray Clay (CH)	Undrained	90	95	0.00028	0.000028	0.1684	0.03	0.15	0.63	1.24	0.001	22	1.1

ID	Name	Type	EA [lb/ft]	EI [lbft^2/ft]	w [lb/ft^2]	nu [-]	M_p [lbft/ft]	N_p [lb/ft]
1	I-wall	Elastic	6.32E+08	54290000	150	0.22	1.00E+15	1.00E+15
2	Sheetpile (Z-22)	Elastic	1.87E+08	16400000	22	0.22	1.00E+15	1.00E+15

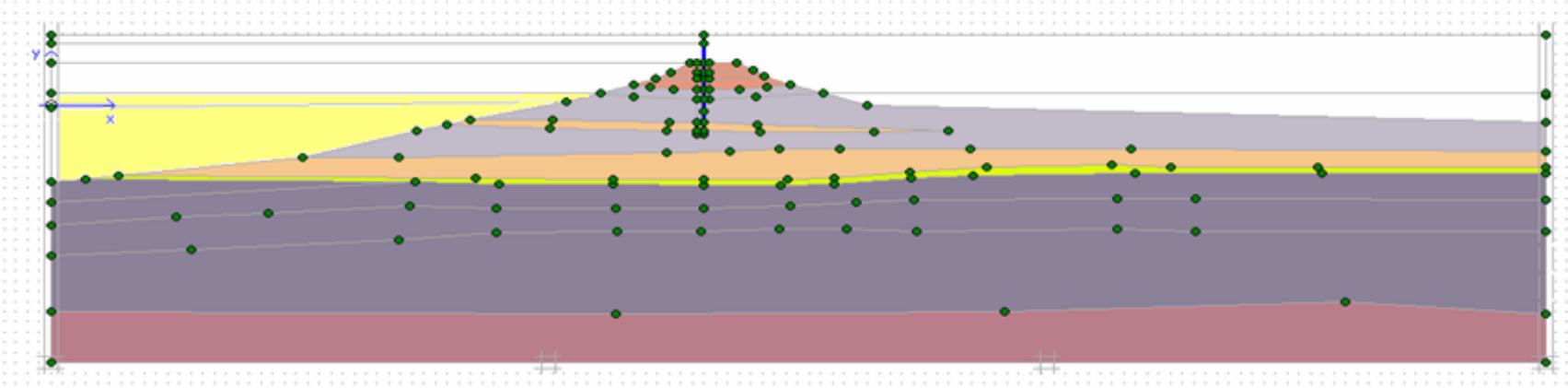

Figure 6.27: Geometry and input parameters for FEM (PLAXIS) stability analyses for Lower Ninth Ward, IHNC East Bank, South Breach.

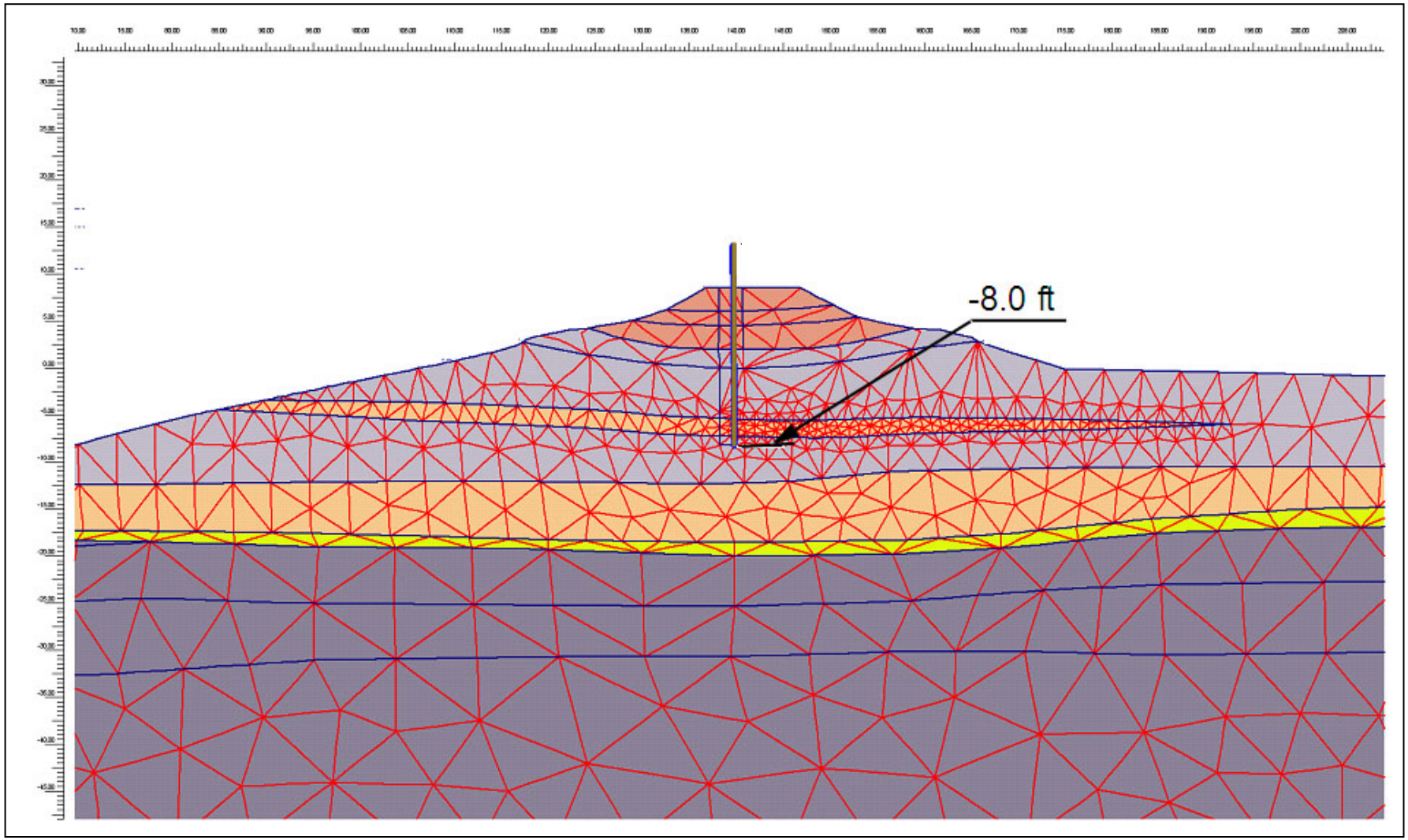

Figure 6.28: Deformed mesh after modeling staged construction for the levee and allowing for consolidation for Lower Ninth Ward, IHNC East Bank, South Breach.

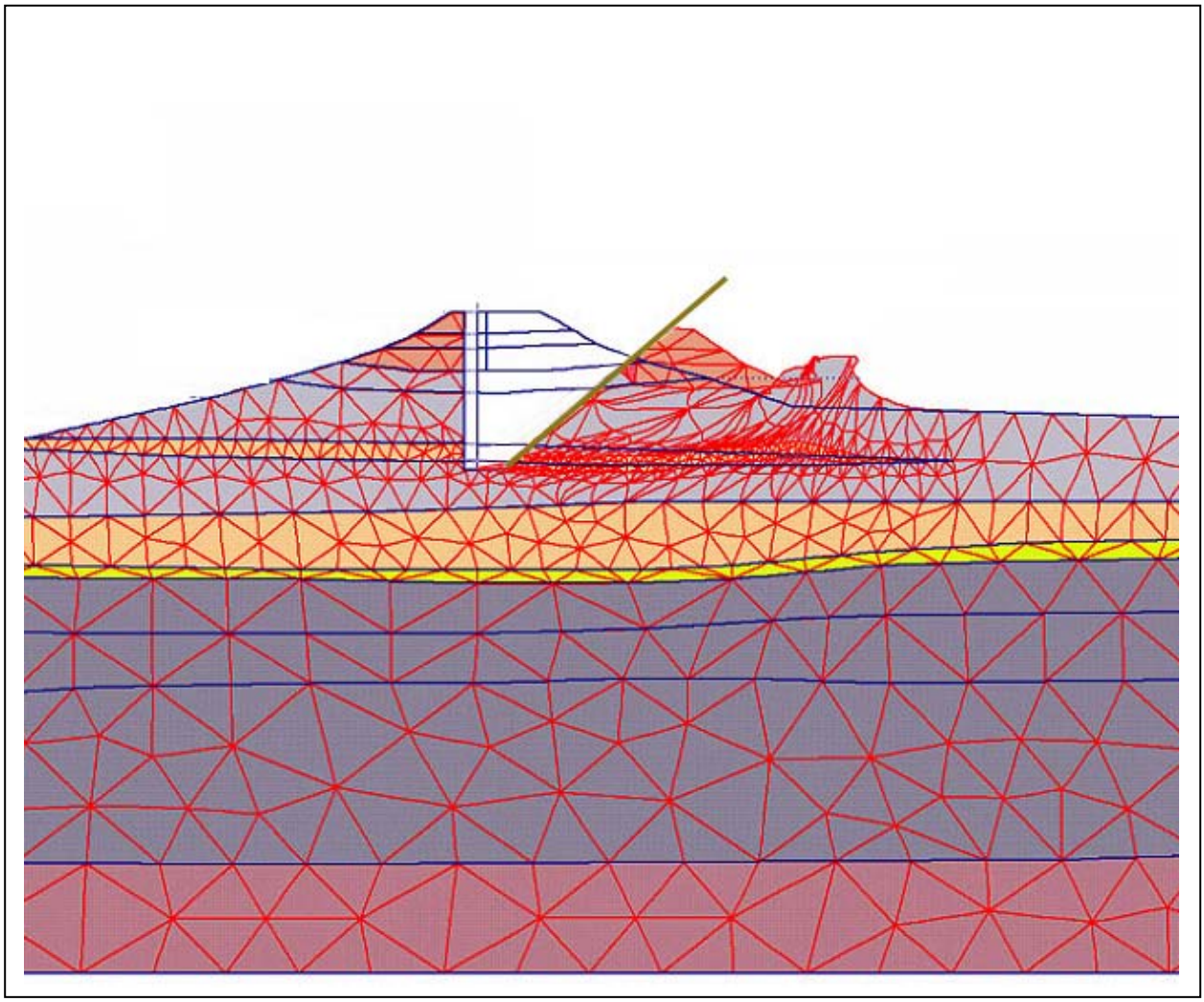

Figure 6.29: Deformed mesh for storm surge elevation of +13.5ft (MSL) for Lower Ninth Ward, East Bank, South Breach.

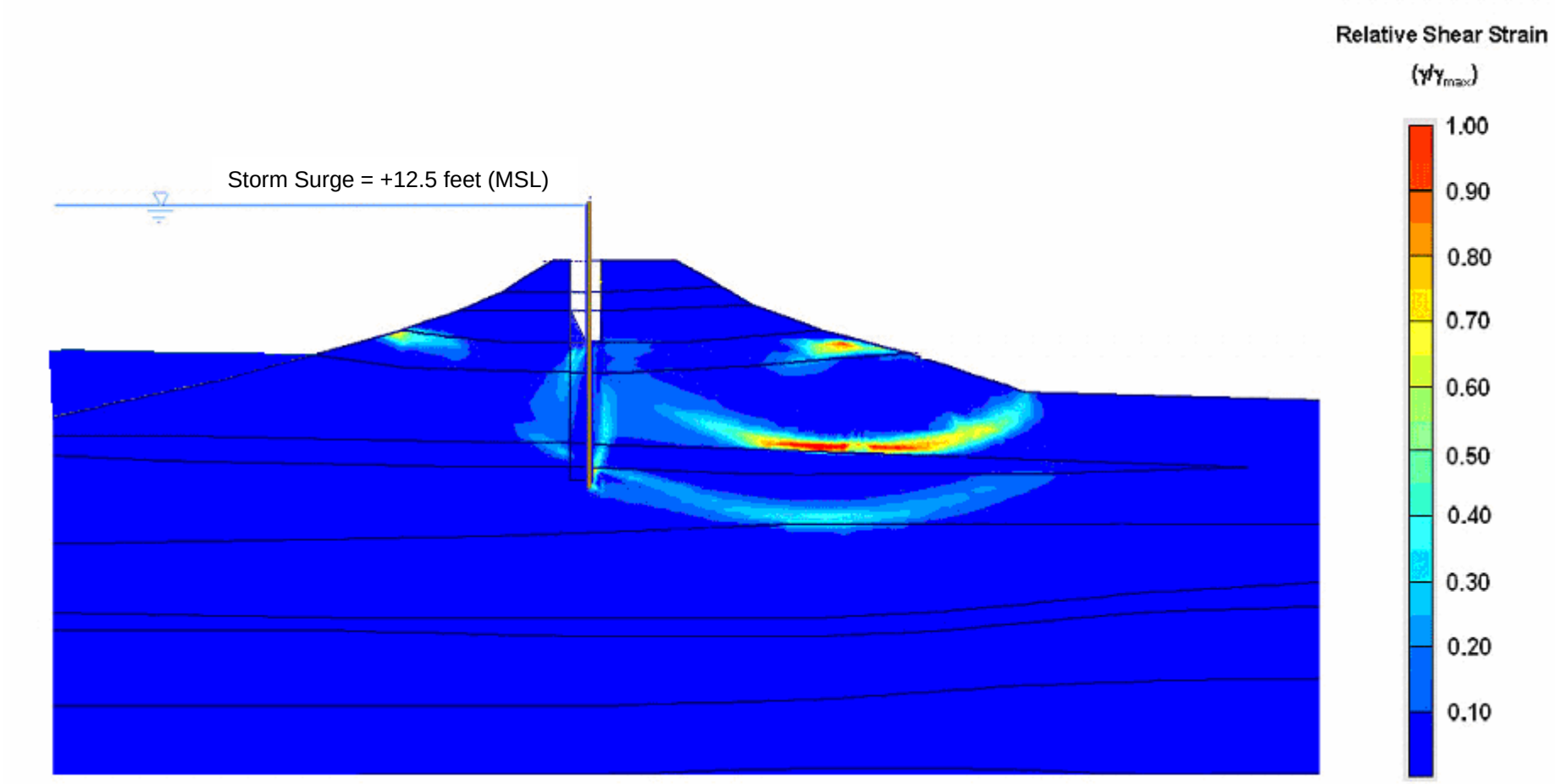

Figure 6.30: Normalized shear strain contours (shear strain divided by strain to failure) for a storm surge at Elev. + 12.5 feet (MSL) at the Lower Ninth Ward, IHNC East Bank, South breach site; gapping at outboard toe of floodwall is developed fully through the embankment fill material.

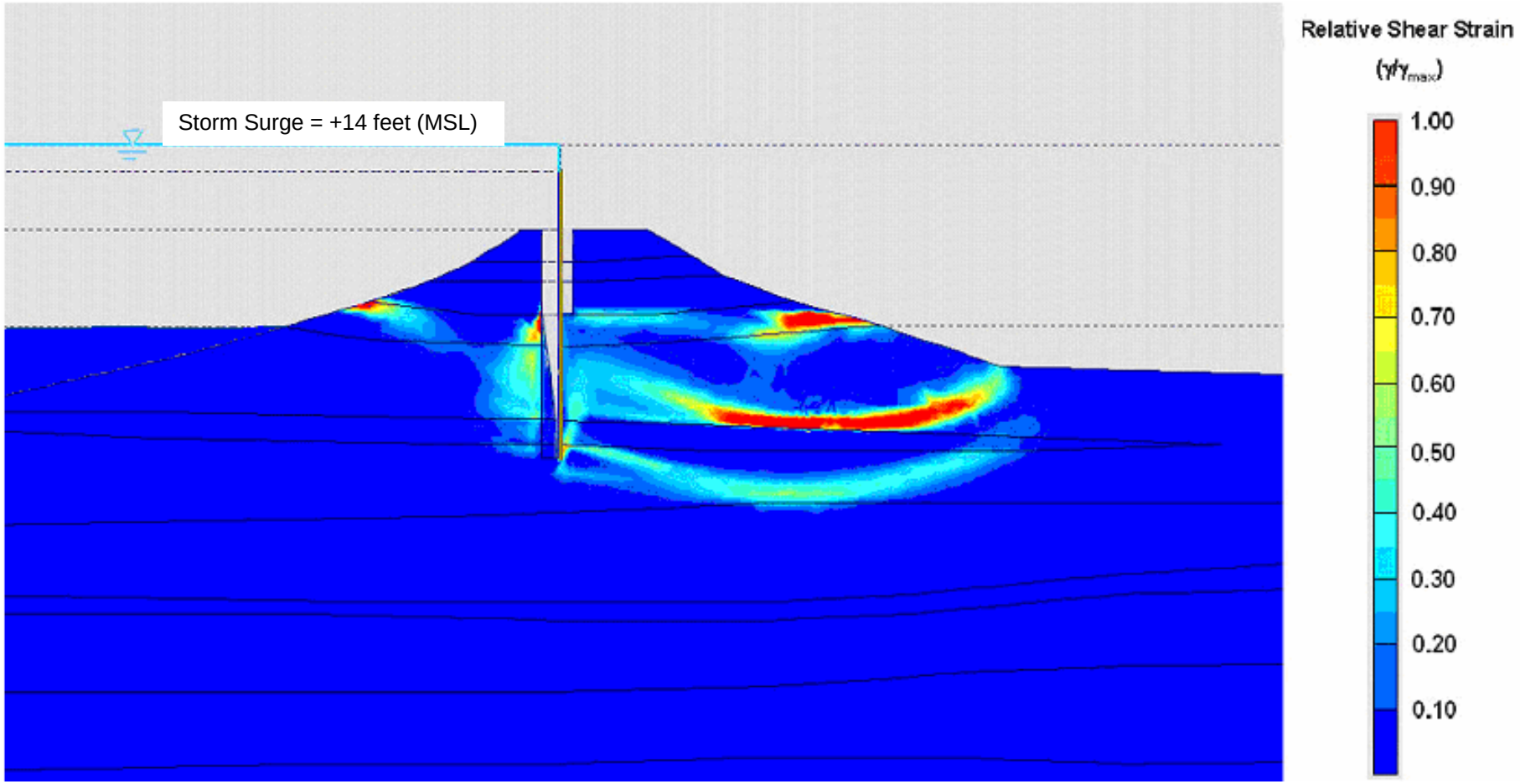

Figure 6.31: Normalized shear strain contours (shear strain divided by strain to failure) for a storm surge at Elev. + 14 feet (MSL) at the Lower Ninth Ward, IHNC East Bank, South breach site; gapping at outboard toe of floodwall is fully developed.

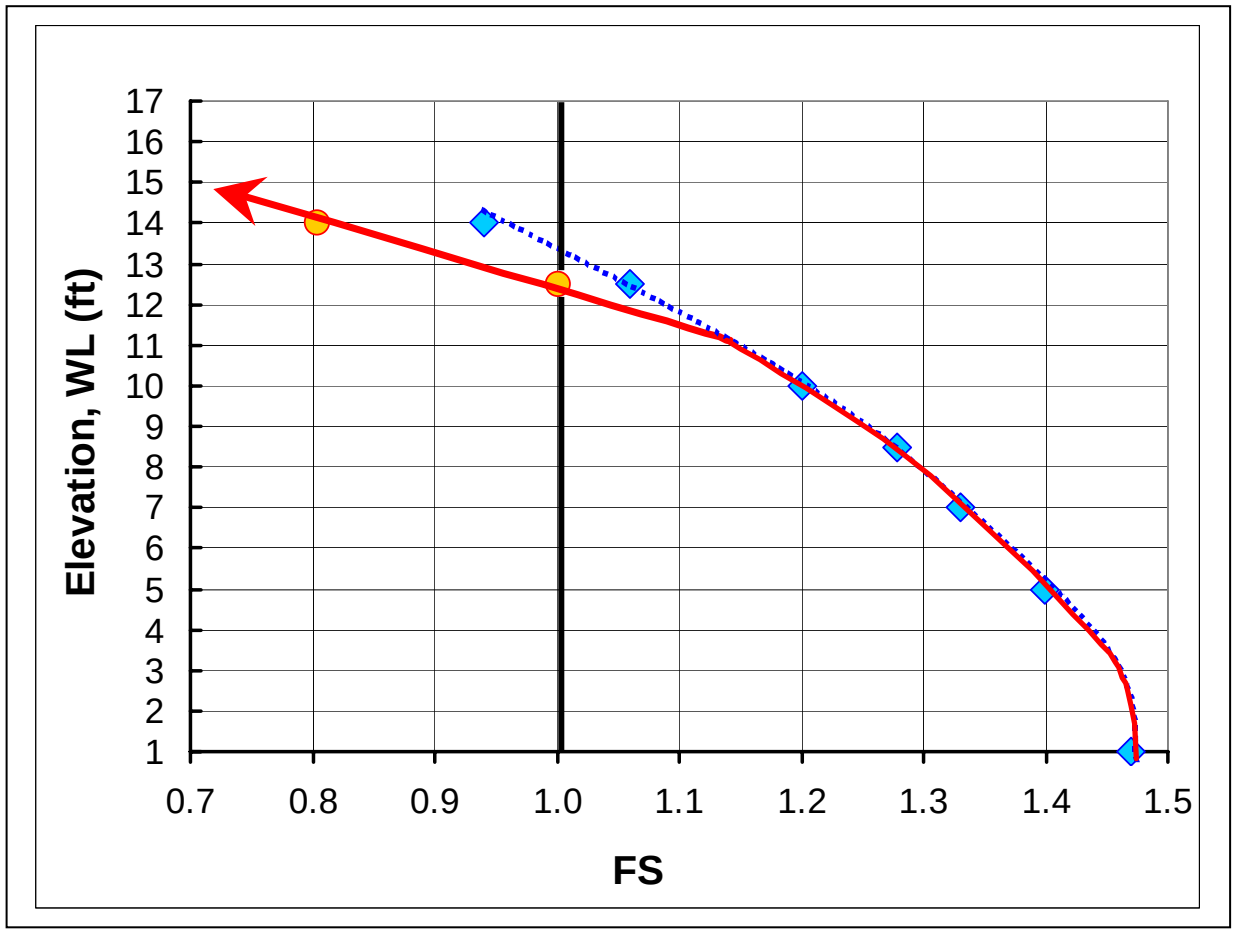

Figure 6.32: Calculated Factors of Safety for two modes based on PLAXIS analyses of the Lower Ninth Ward South breach site (east bank IHNC) for various canal water elevations; showing the best-estimated path to failure.

	PARAMETER						
MATERIAL	γ (pcf)	ϕ	c (psf)	Kh (ft/hr)	Kh (cm/s)	Kv/Kh	Θ *
Fill	105	0	900	1.17E-04	9.91E-07	1	0.35
Upper CH	95	0	800	2.00E-04	1.69E-06	0.333	0.35
Upper Marsh	85	28	0	1.10E+00	9.31E-03	0.25	0.5
OC Grey CH	95	0	500	2.00E-04	1.69E-06	0.333	0.35
NC Grey CH	95	0	Su/p: 0.28	2.00E-04	1.69E-06	0.333	0.35
Lower Marsh	85	28	0	1.10E+00	9.31E-03	0.25	0.5
Silt	110	0	600	1.17E-04	9.91E-07	0.333	0.41
Lean Clay	100	0	600	2.00E-04	1.69E-06	0.333	0.38
Sands	120	30	0	1.00E+00	8.5E-03	0.5	0.42
Gaps				100		10	1

* Fredlund et al, Green and Corey, Van Genuchten

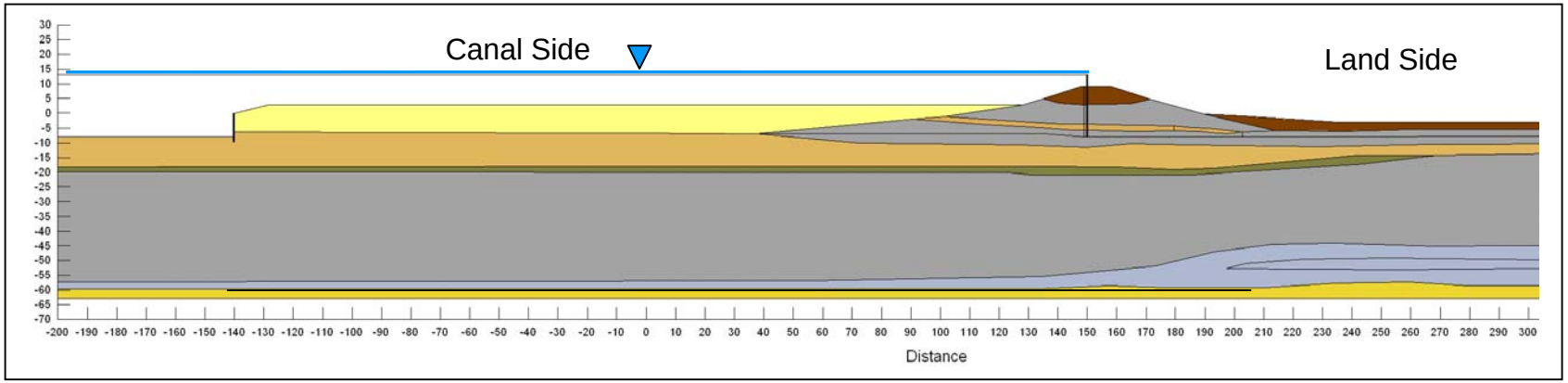

Figure 6.33: Geotechnical cross-section for analysis of the IHNC east bank, south breach.

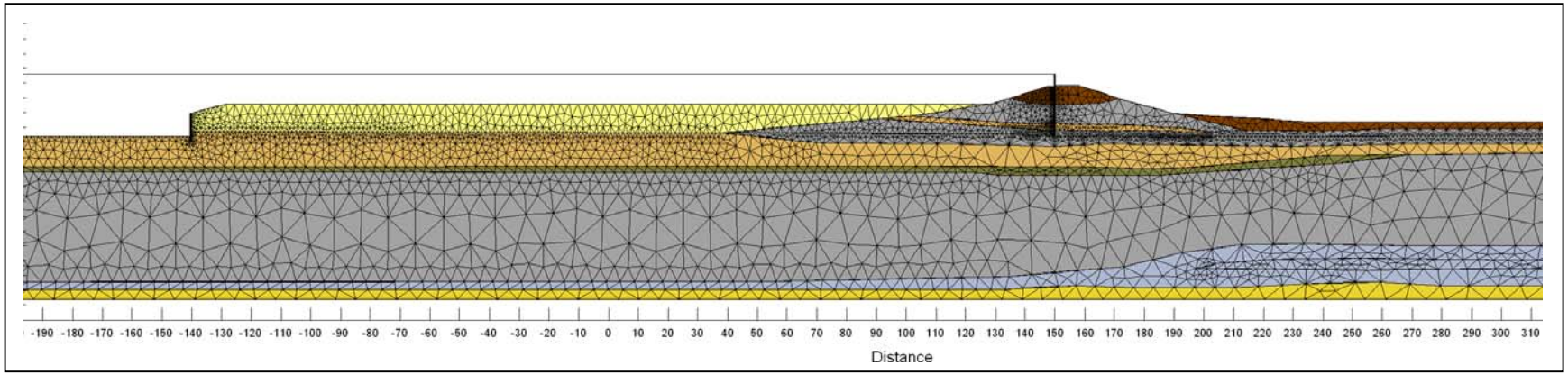

Figure 6.34: Finite difference mesh for seepage analyses for IHNC east bank, south breach.

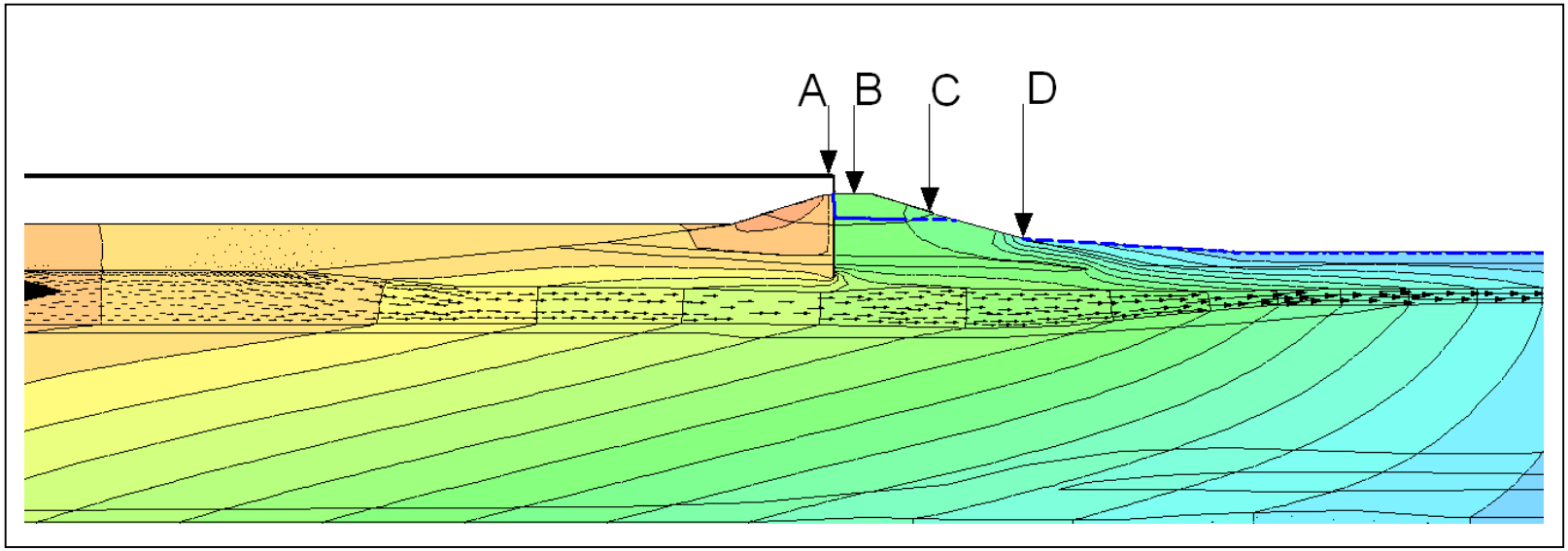

Figure 6.35: Flow net for the south breach on IHNC; storm surge at 14.4ft (MSL). Head contours at 1-foot intervals of head.

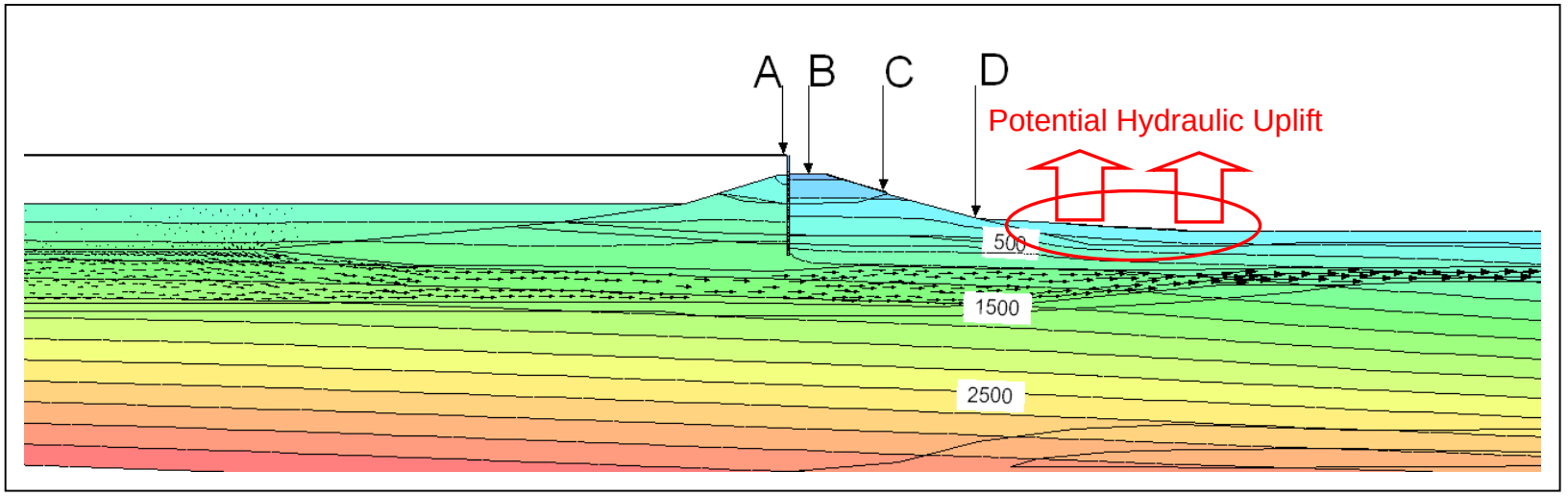

Figure 6.36: Pressure contours for the south breach on IHNC. Storm surge at 14.4ft (MSL).

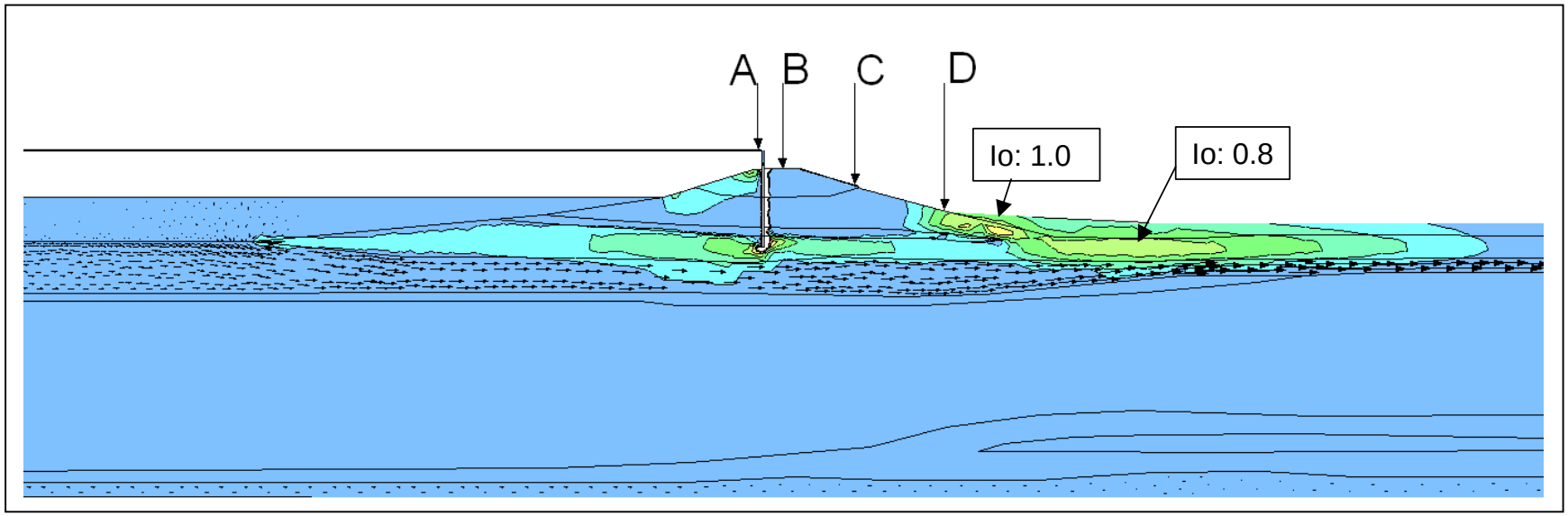

Figure 6.37: Hydraulic gradients for the south breach on IHNC east bank; storm surge at 14.4ft (MSL). Maximum exit gradient at the levee toe is $i_o \approx 0.8$ to 1.0.

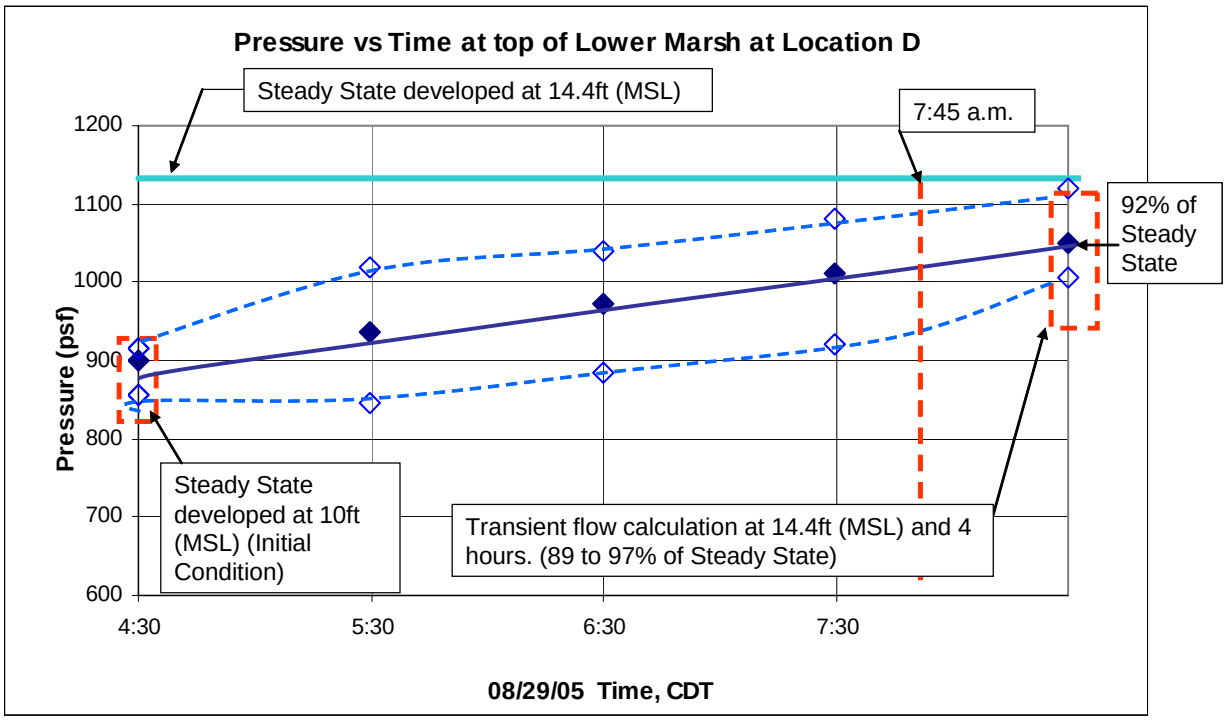

Figure 6.38: Transient flow pore pressure generation for the south breach on IHNC east bank.

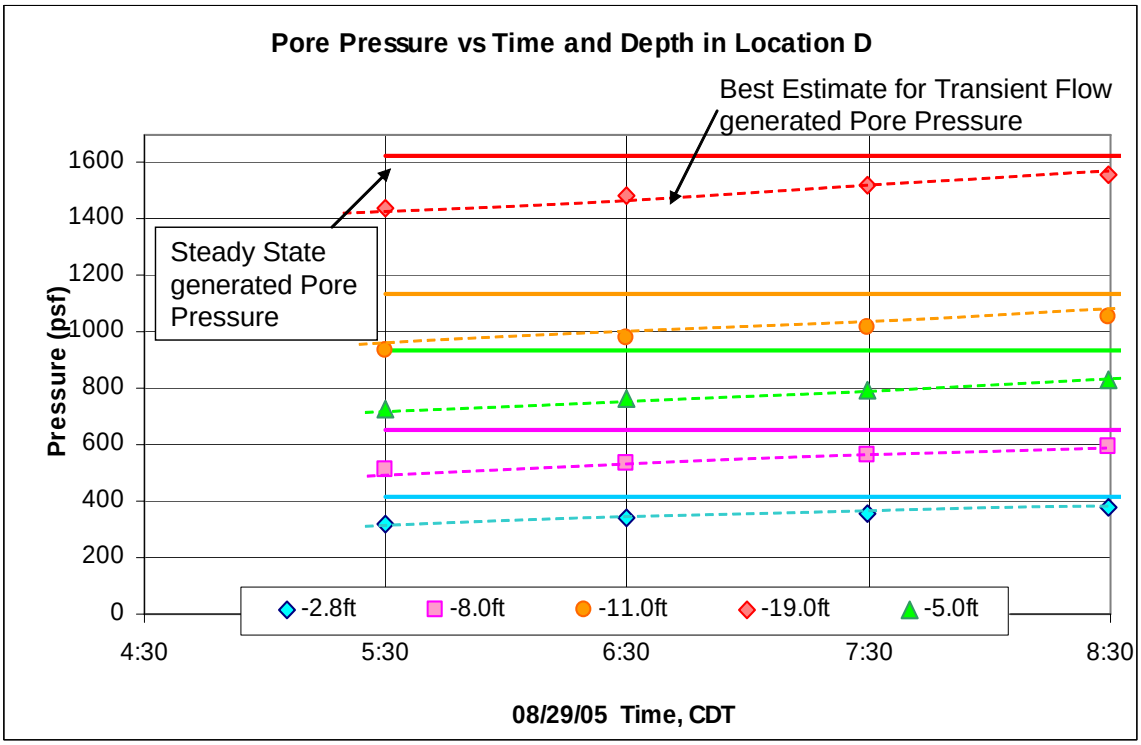

Figure 6.39: Pore pressure generation at different times and depths at the inboard toe of the south breach on IHNC east bank.

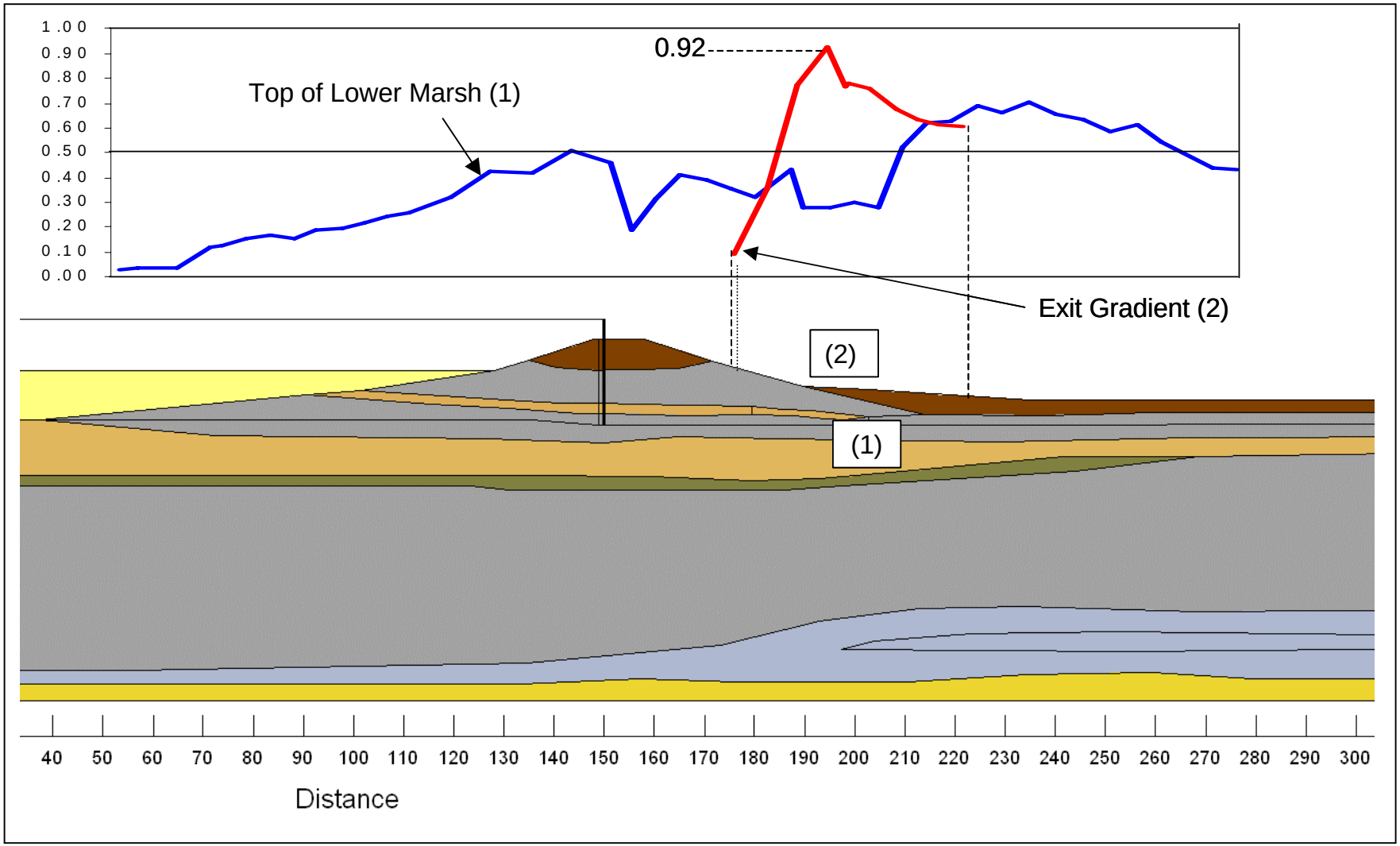

Figure 6.40: Hydraulic gradients at the south breach on IHNC east bank.

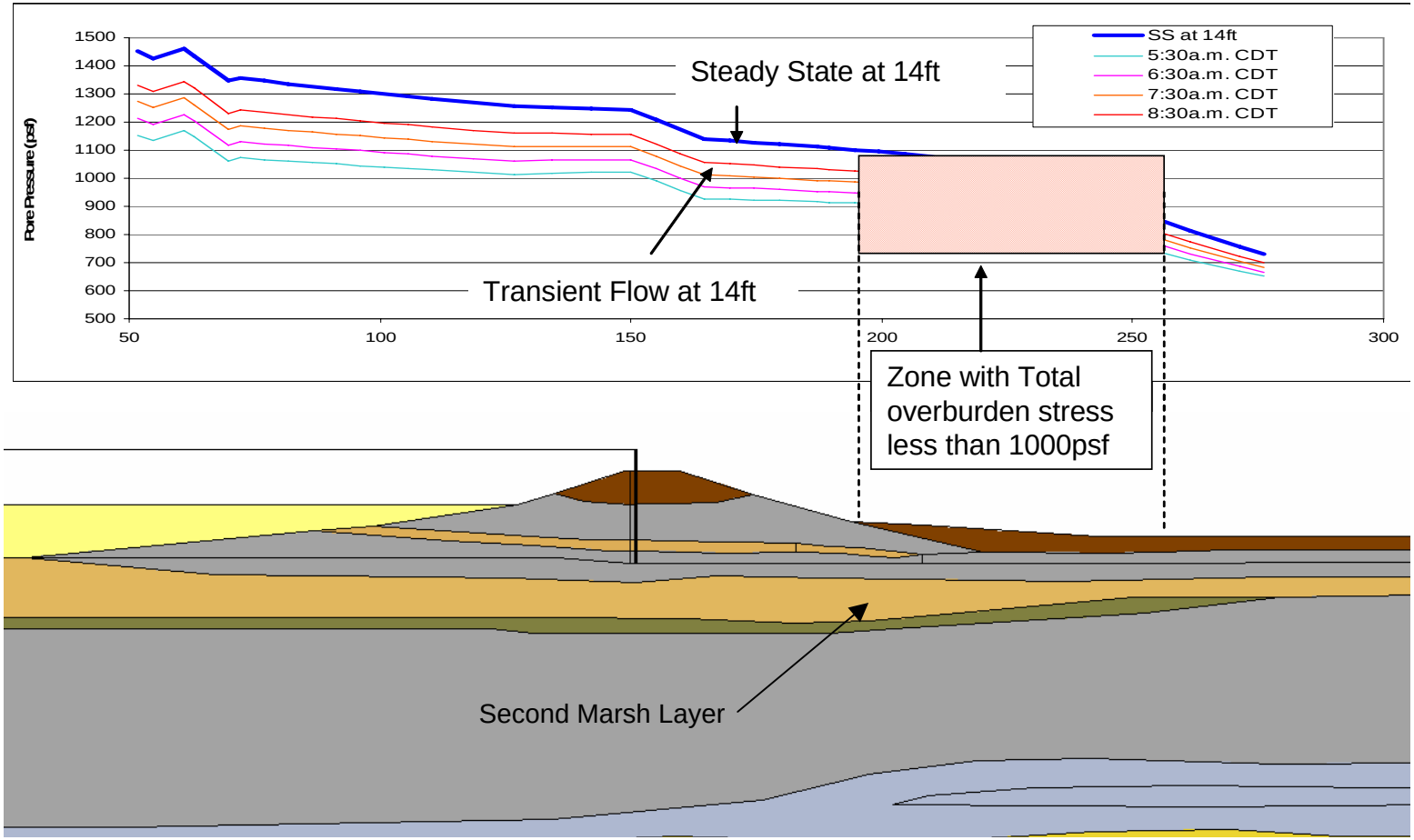

Figure 6.41: Pore pressure versus horizontal distance and time at the top of the second marsh layer; south breach on IHNC east bank.

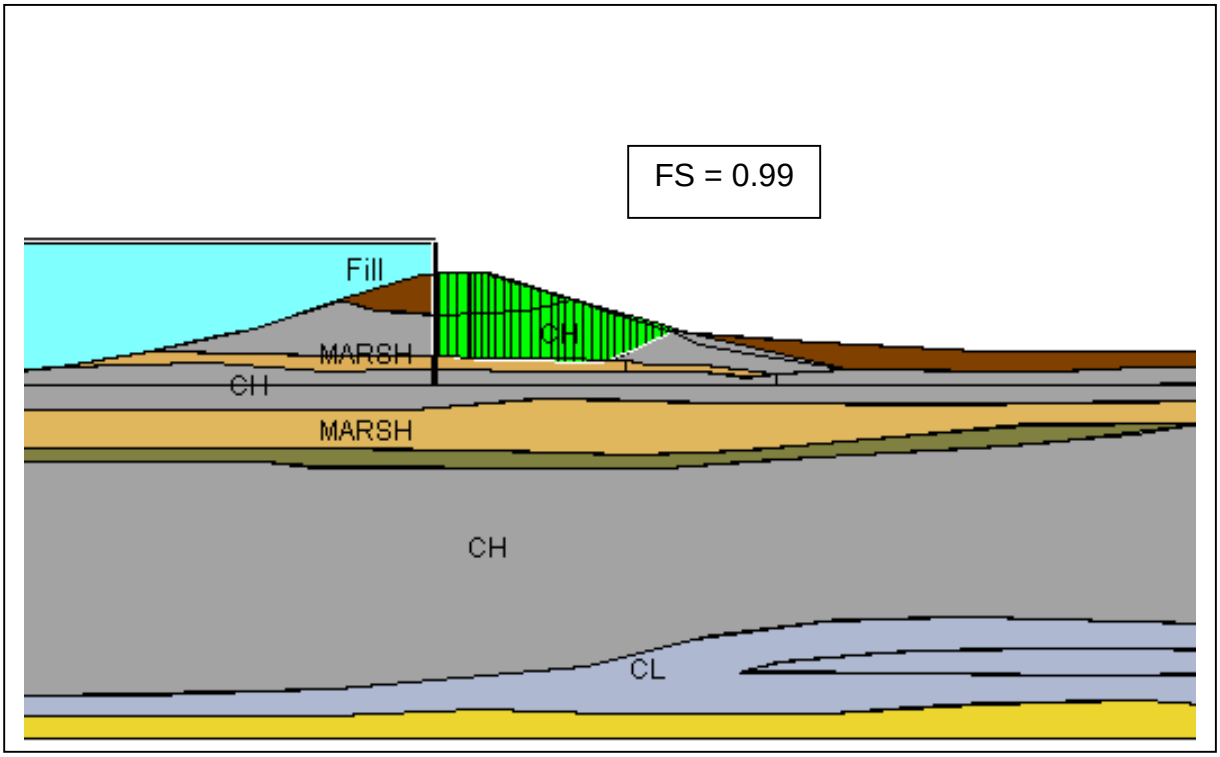

Figure 6.42: Critical failure surface for the south breach on IHNCeast bank; storm surge at 14ft (MSL), failure through upper marsh layer with gap at front of sheetpiles fully developed.

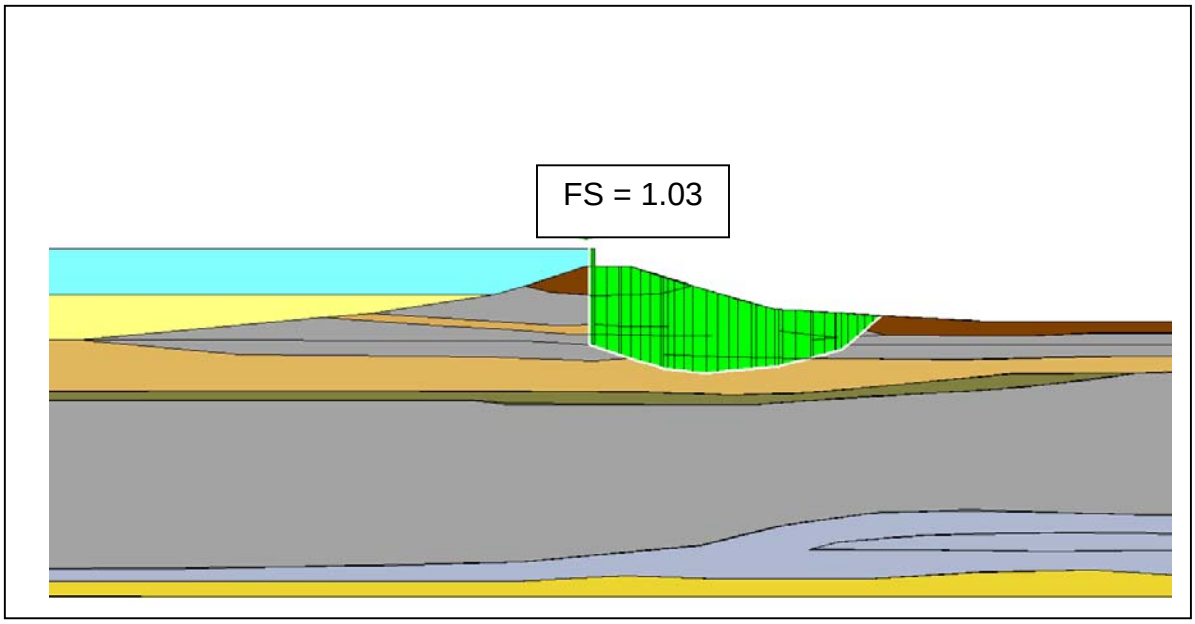

Figure 6.43: Deeper failure surface for the south breach on IHNCeast bank; storm surge at 14ft (MSL), gap at front of sheetpiles fully developed.

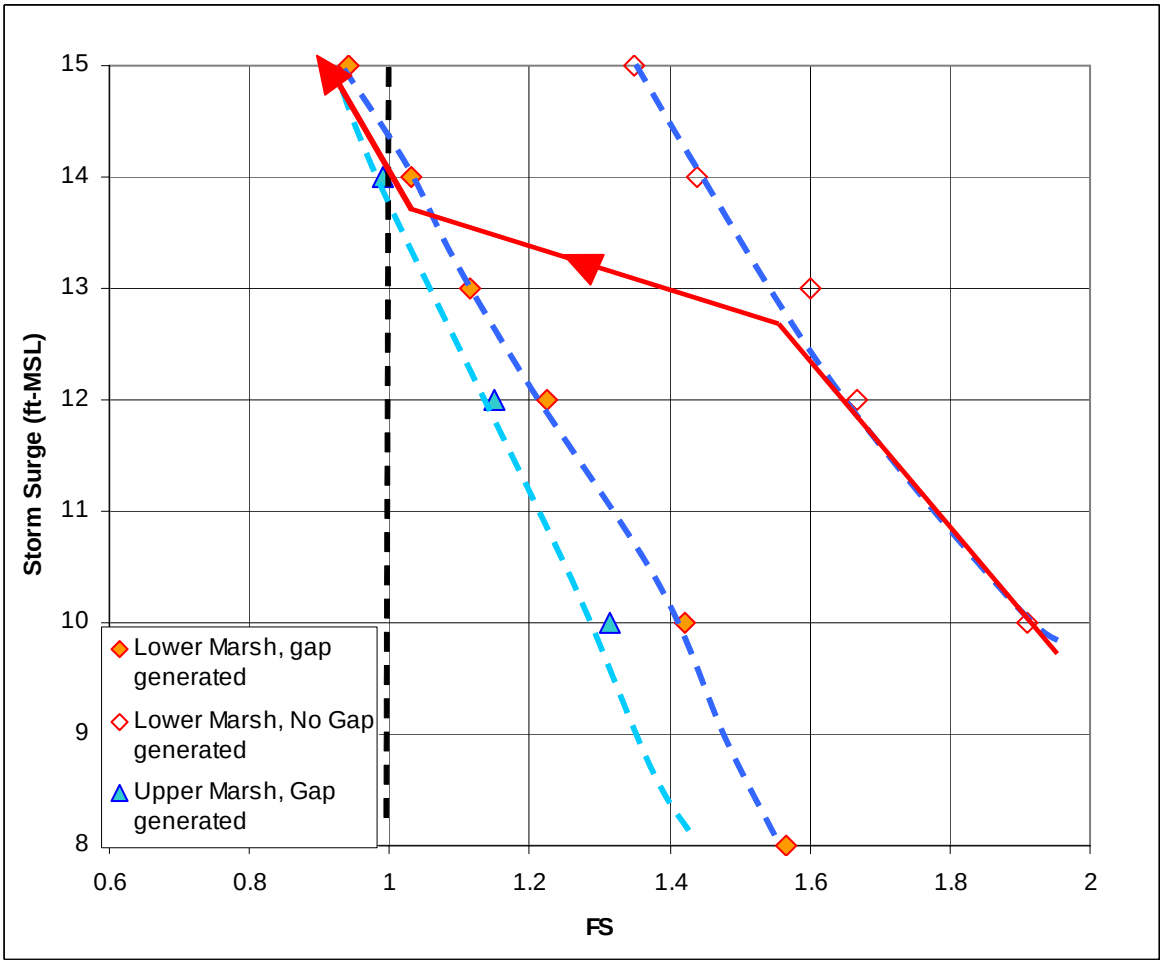

Figure 6.44: Calculated Factors of Safety for three modes based on SLOPE/W analyses of the Lower Ninth Ward South breach site (east bank IHNC) for various canal water elevations; showing the best-estimated path to failure.

Figure 6.45: Aerial view of the south breach at the east bank of the IHNC (at the west end of the Ninth Ward), showing the crevasse splay generated by reverse drainage flow.

[Photograph by U.S. Army Corps of Engineers]

Figure 6.46: Aerial view of the partially repaired north breach on the east bank of the IHNC at the west end of the Lower Ninth Ward.

	PARAMETER						
MATERIAL	**γ (pcf)**	**ϕ**	**c (psf)**	**Kh (ft/hr)**	**Kh (cm/s)**	**Kv/Kh**	**Θ ***
Fill	105	0	900	1.17E-04	9.91E-07	1	0.35
CH	95	0	800	2.00E-04	1.69E-06	0.333	0.35
OC Grey CH	95	0	500	2.00E-04	1.69E-06	0.333	0.35
NC Grey CH	95	0	Su/p: 0.28	2.00E-04	1.69E-06	0.333	0.35
Marsh	85	28	0	1.10E+00	9.31E-03	0.25	0.5
Lean Clay	100	0	600	2.00E-04	1.69E-06	0.333	0.38
Sands	120	30	0	1.00E+00	8.5E-03	0.5	0.42
Gaps				100		10	1

* Fredlund et al, Green and Corey, Van Genuchten

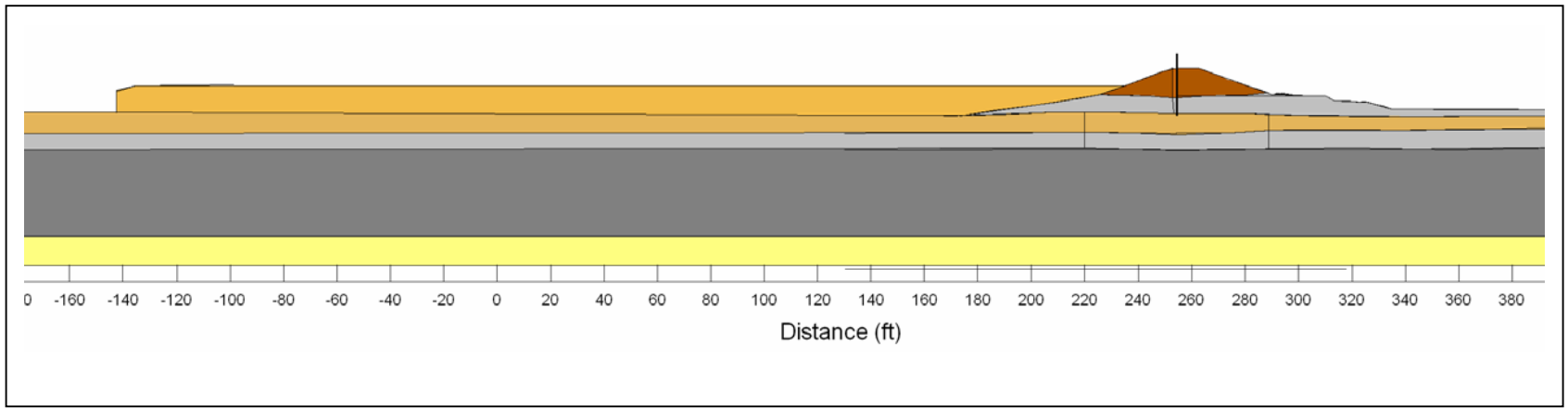

Figure 6.47: Geotechnical cross-section for analysis of the IHNC east bank, north breach.

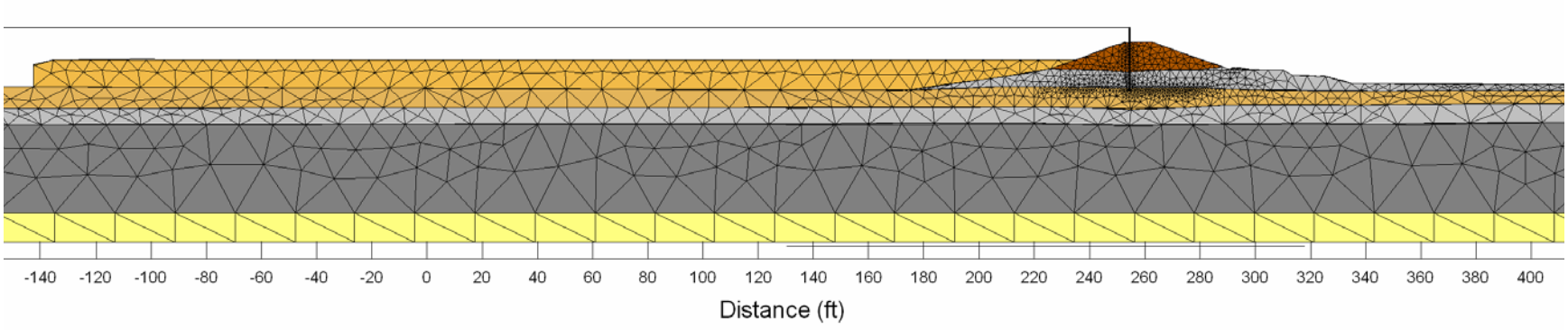

Figure 6.48: Finite difference mesh for seepage analyses for IHNC east bank, north breach.

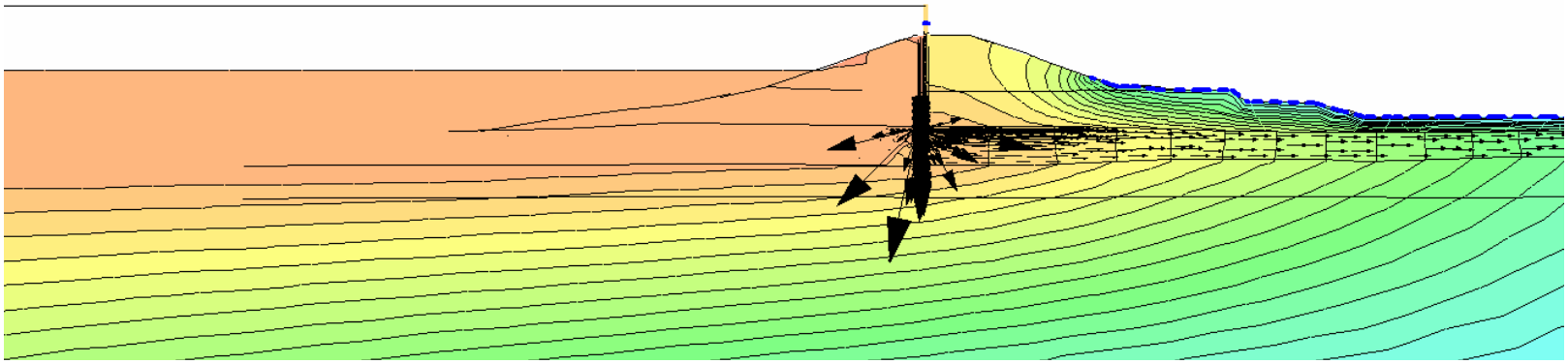

Figure 6.49: Flow net generation for the north breach on IHNC east bank. Storm surge at +14.4ft (MSL). Head contours at 1 foot intervals of hydraulic head.

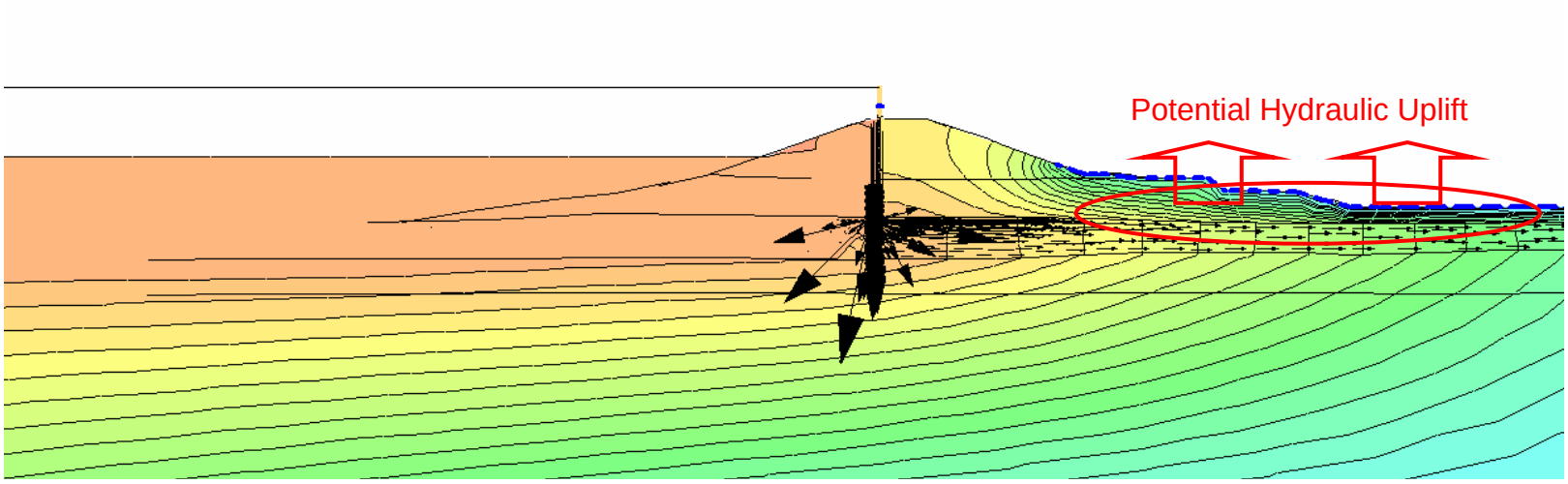

Figure 6.50: Pressure contours for the north breach on IHNC east bank. Storm surge at +14.4ft (MSL). Pore pressure contours at intervals of 62.4 lb/ft^2.

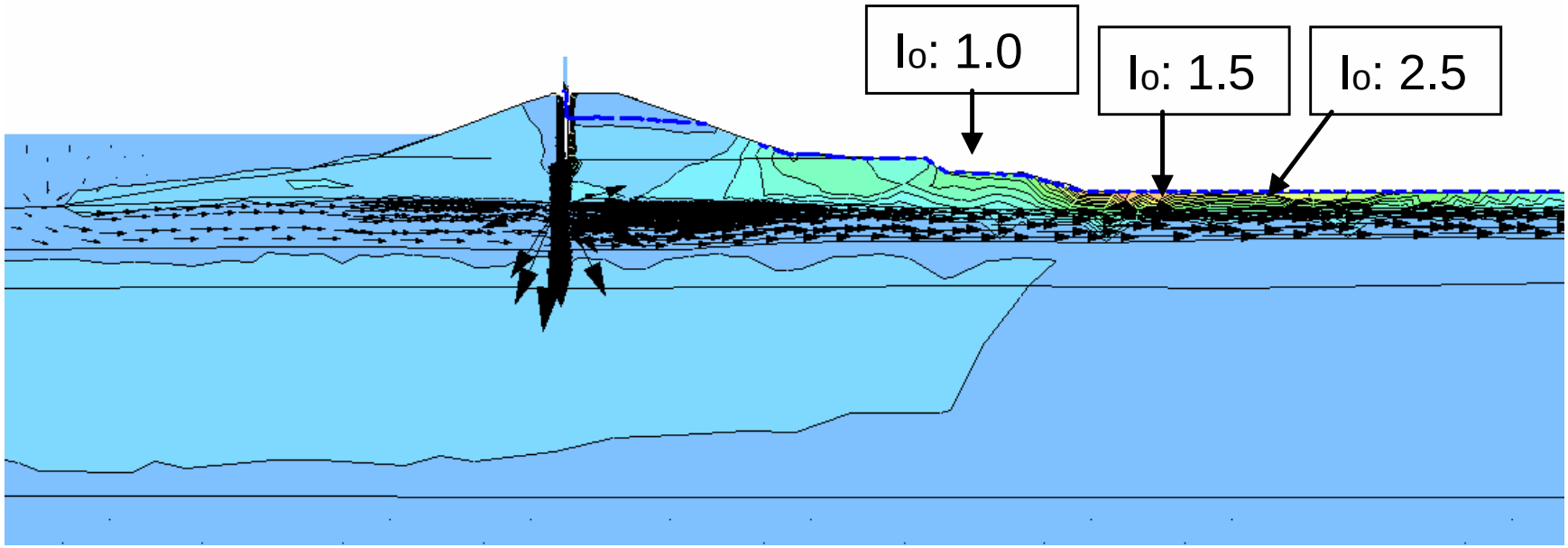

Figure 6.51: Hydraulic gradients for the north breach on IHNC. Storm surge at +14.4ft (MSL). Maximum exit gradient on the upper levee toe is $i_o \approx 1.0$, and $i_o \approx 1.5$ to 2.5 at the lower toe.

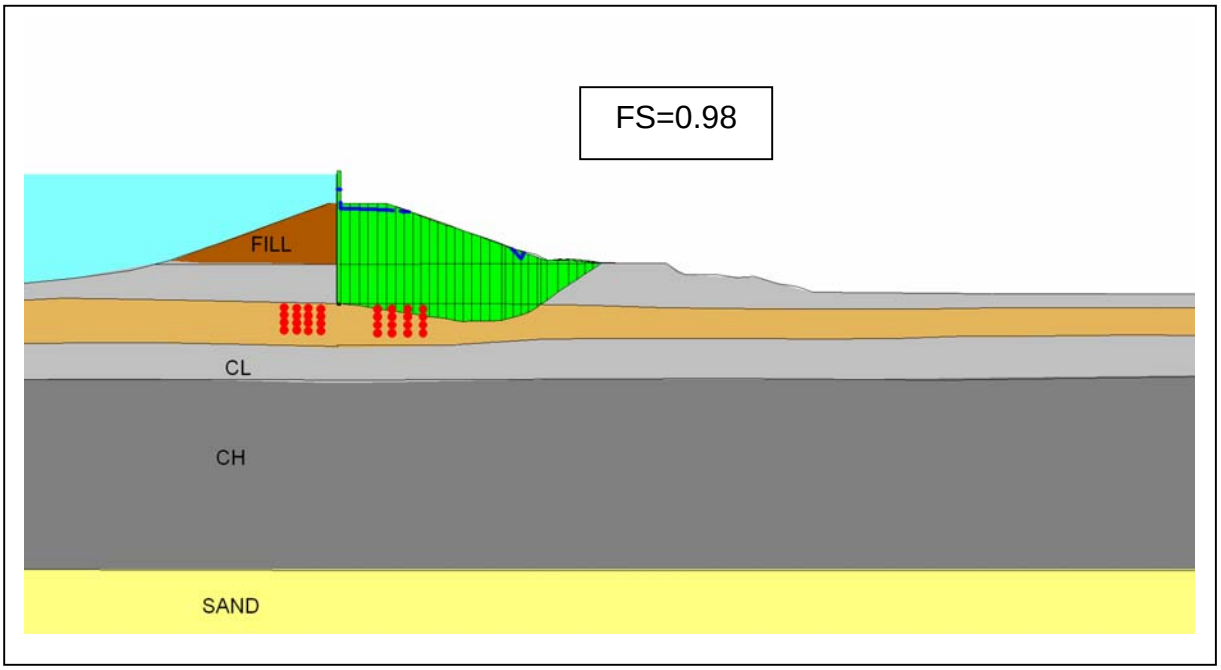

Figure 6.52: Critical potential stability failure surface for the north breach on IHNC. Storm surge at +14 ft (MSL).

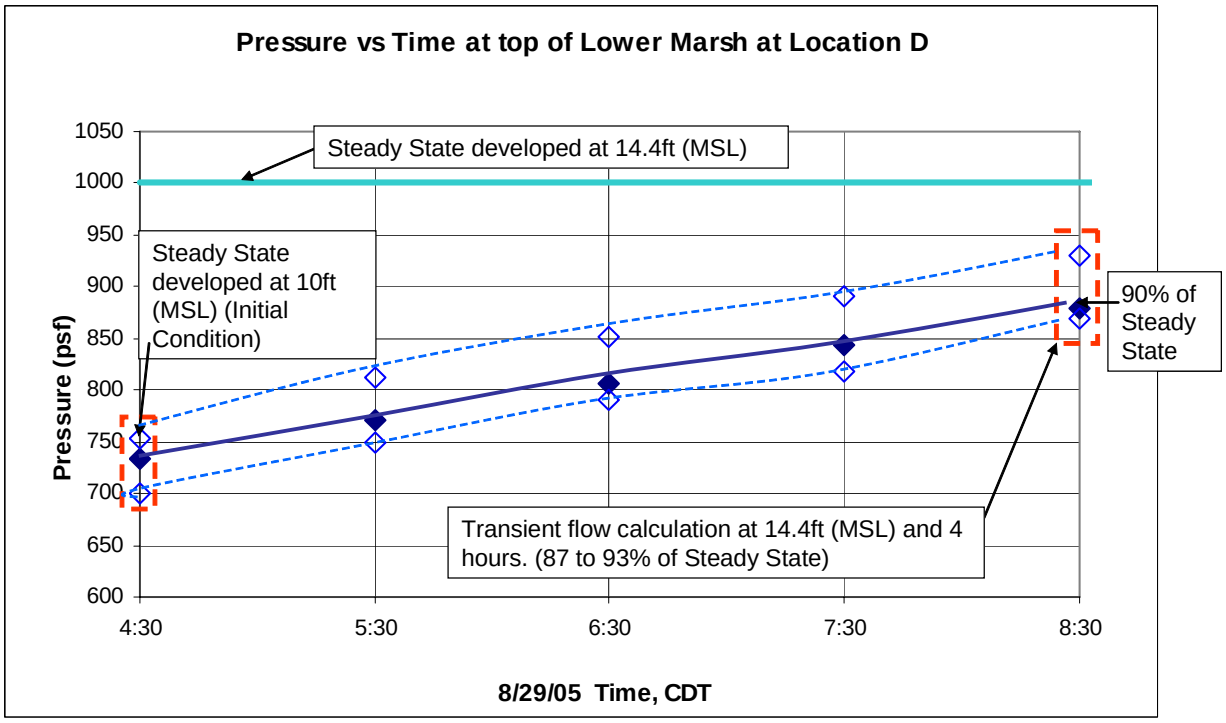

Figure 6.53: Transient flow pore pressure generation for the north breach on IHNC east bank.

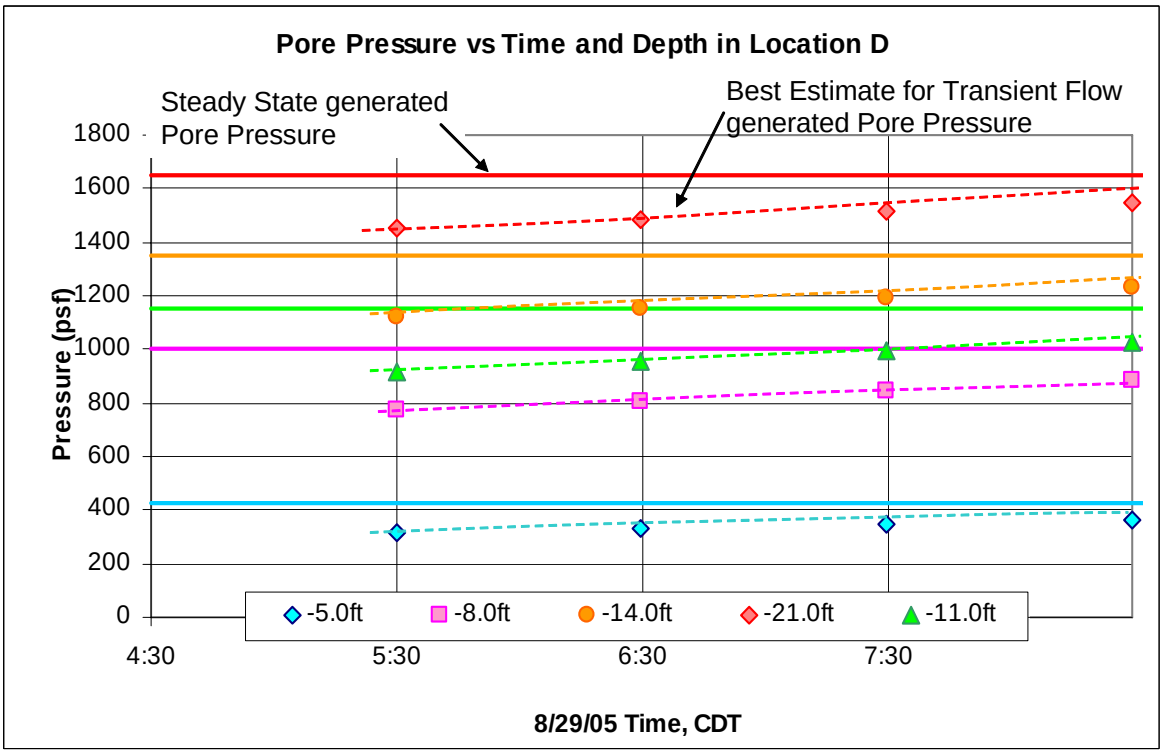

Figure 6.54: Pore pressure generation at different times and depths at the inboard toe of the north breach on IHNC east bank.

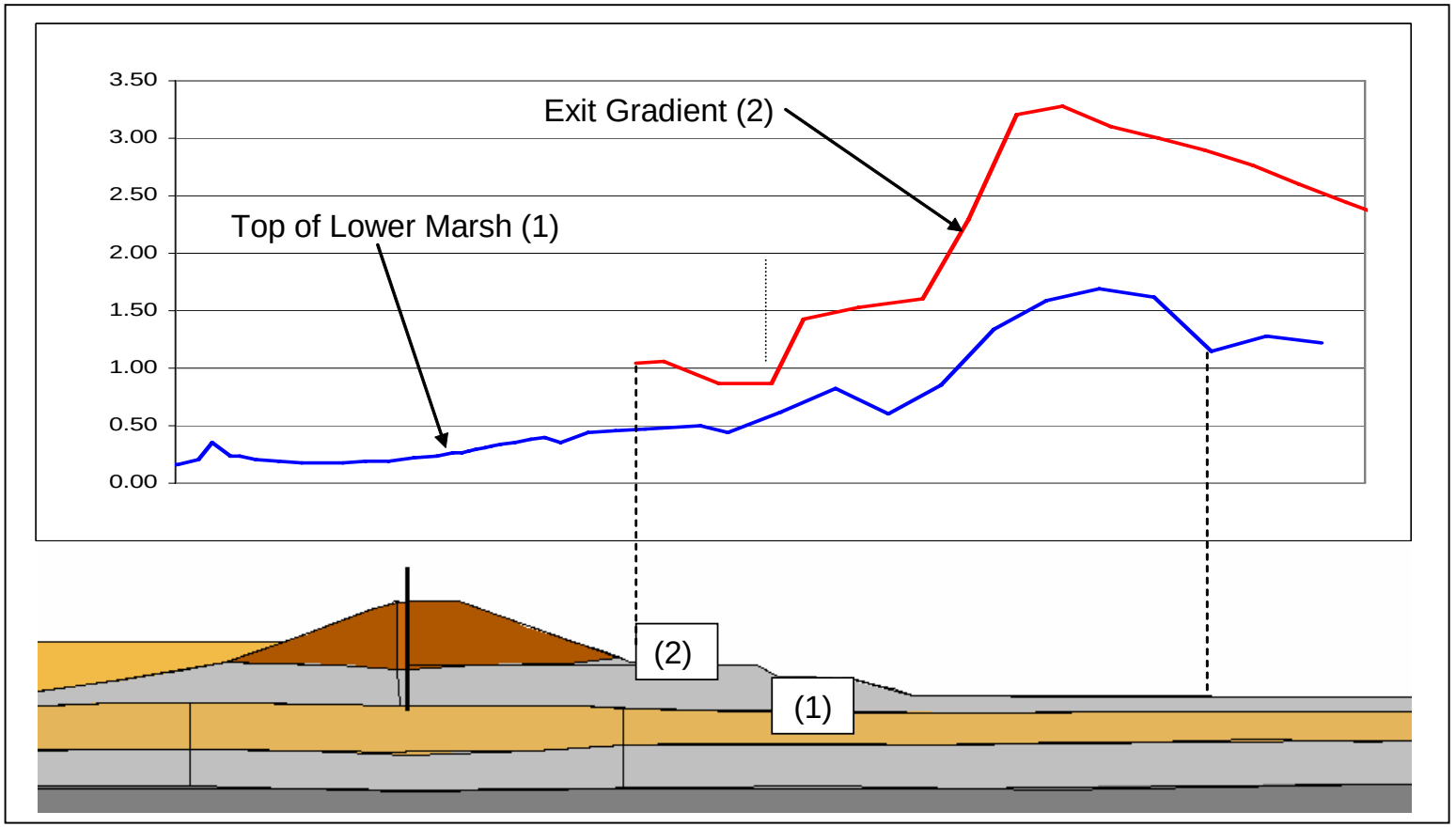

Figure 6.55: Hydraulic gradients on the south breach on IHNC east bank.

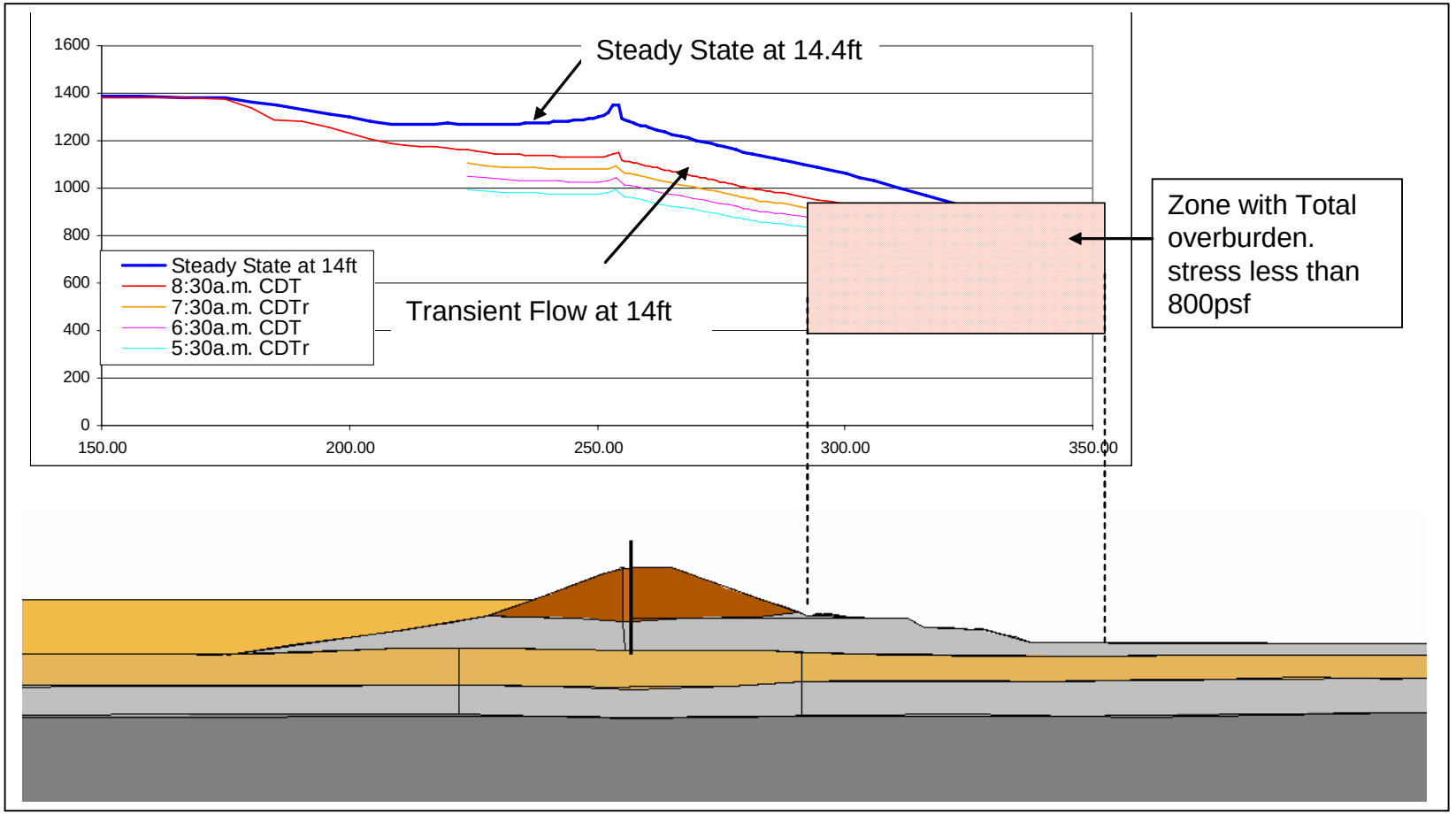

Figure 6.56: Pore pressure versus horizontal distance and time on the north breach on IHNC east bank.

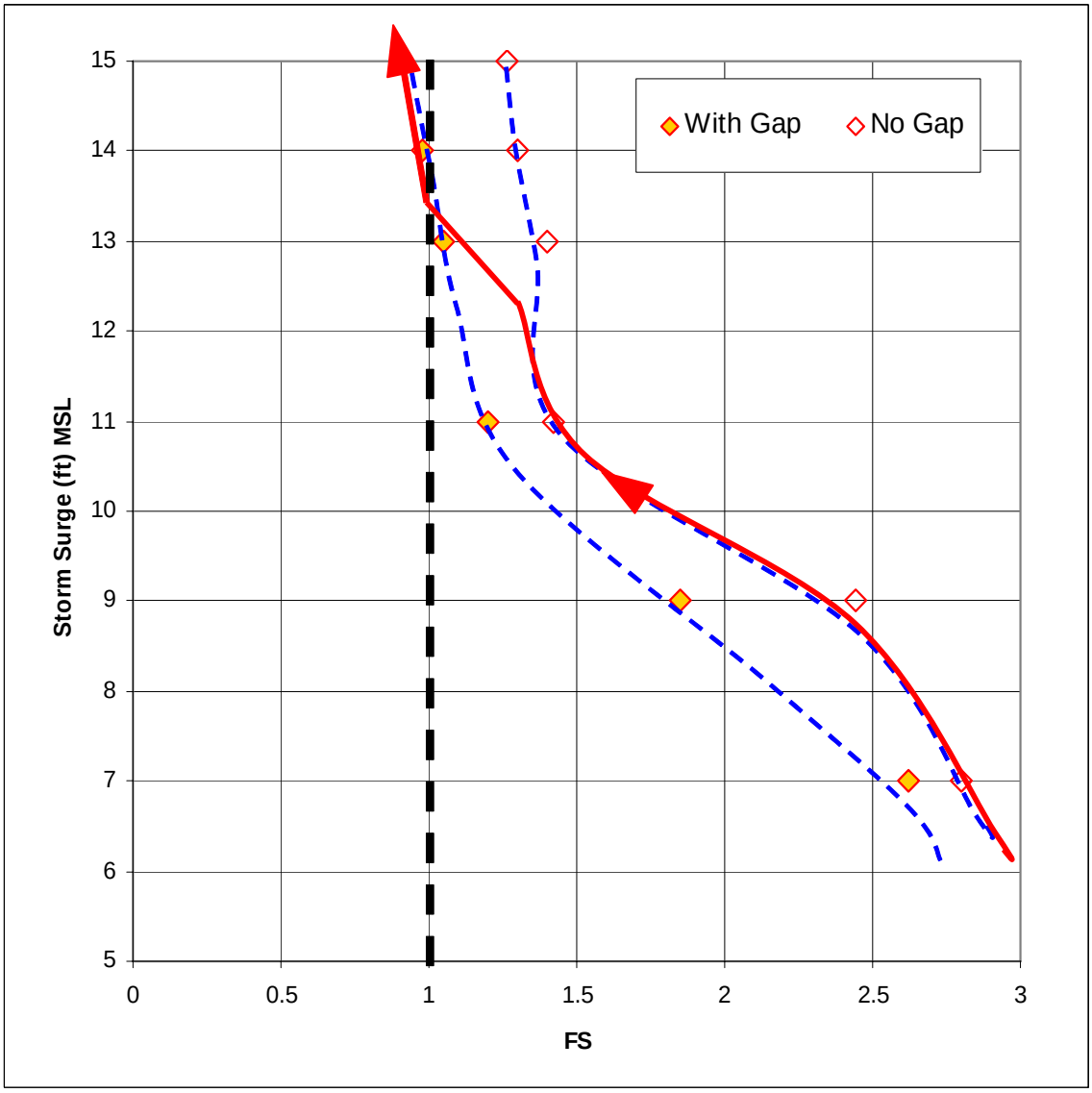

Figure 6.57: Factor of Safety vs. water elevation (ft, MSL) for the north breach, east bank of the IHNC at the west end of the Lower Ninth Ward.

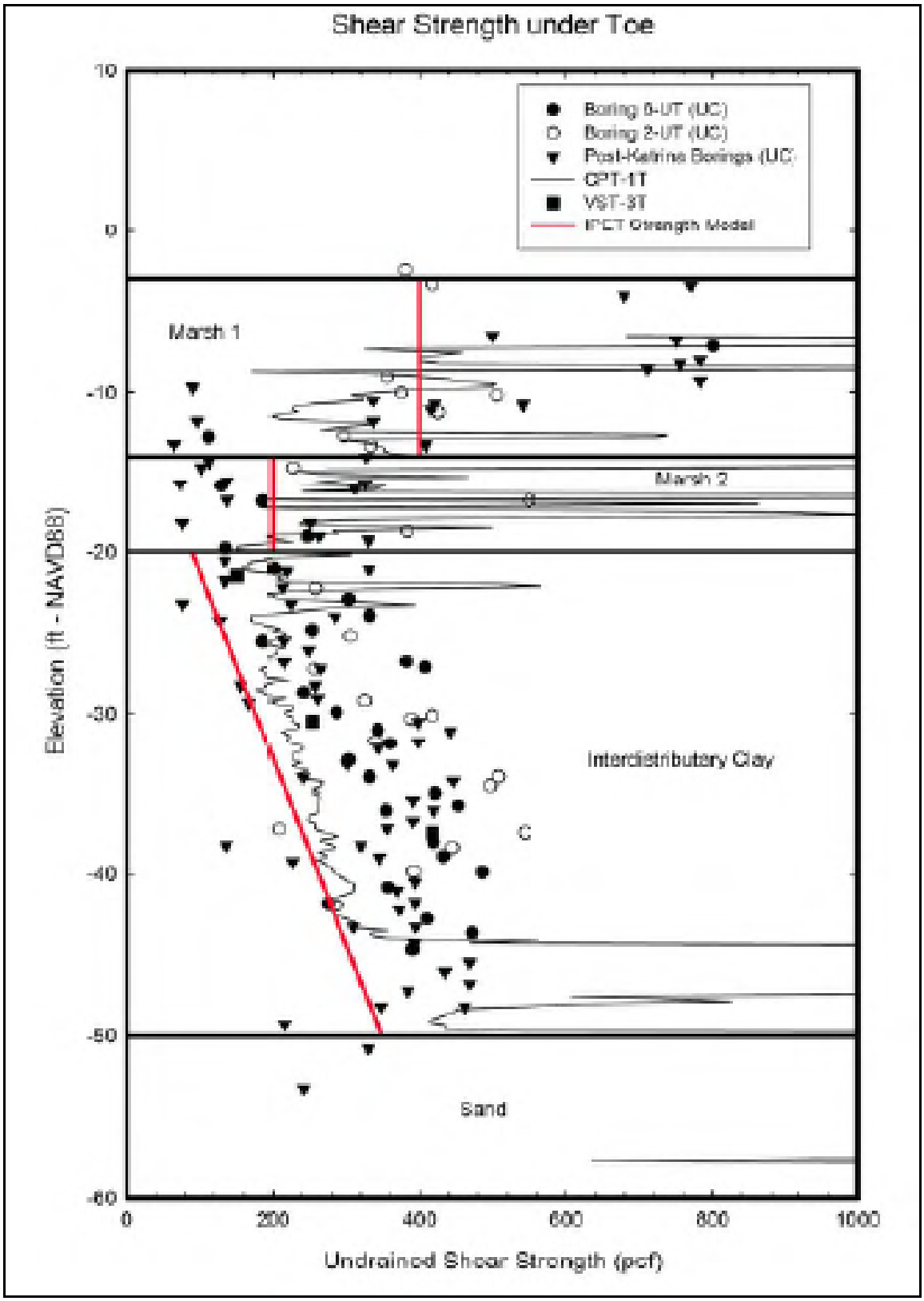

Figure 6.58: IPET shear strength profile; IHNC east bank/Lower Ninth Ward (North) breach.

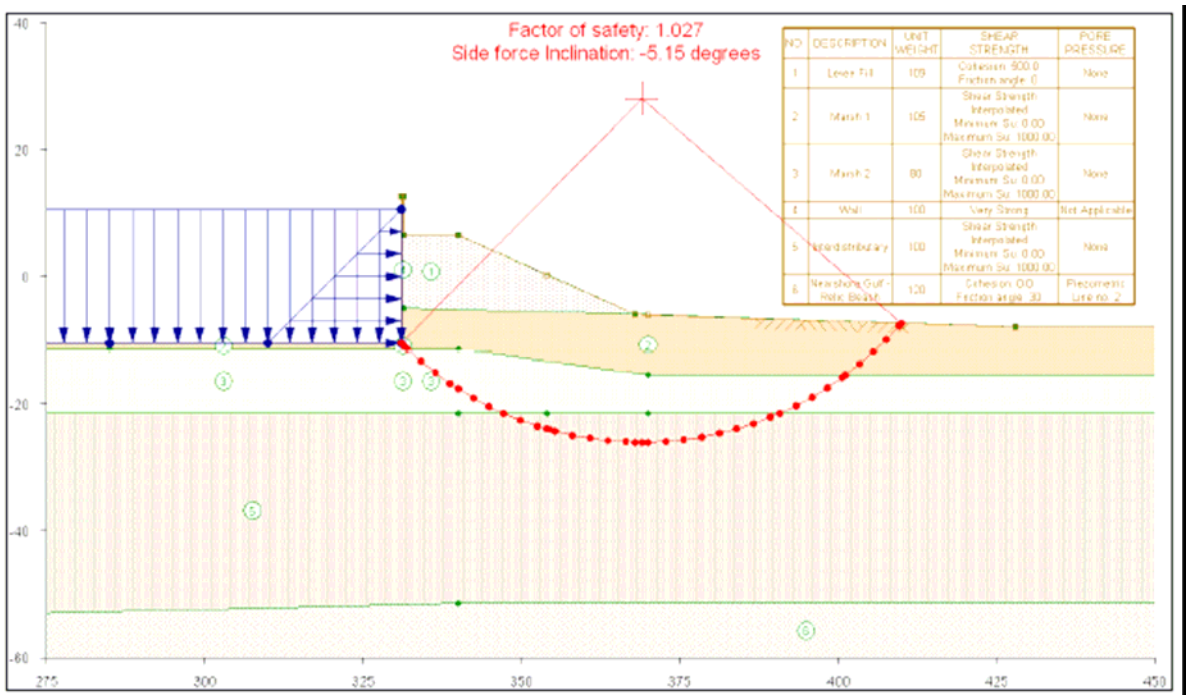

Figure 6.59: Critical limit equilibrium stability failure mode from IPET Draft Final Report; canal water elevation at +9 feet (MSL). Factor of Safety: 1.03.
[IPET; June 1, 2006]

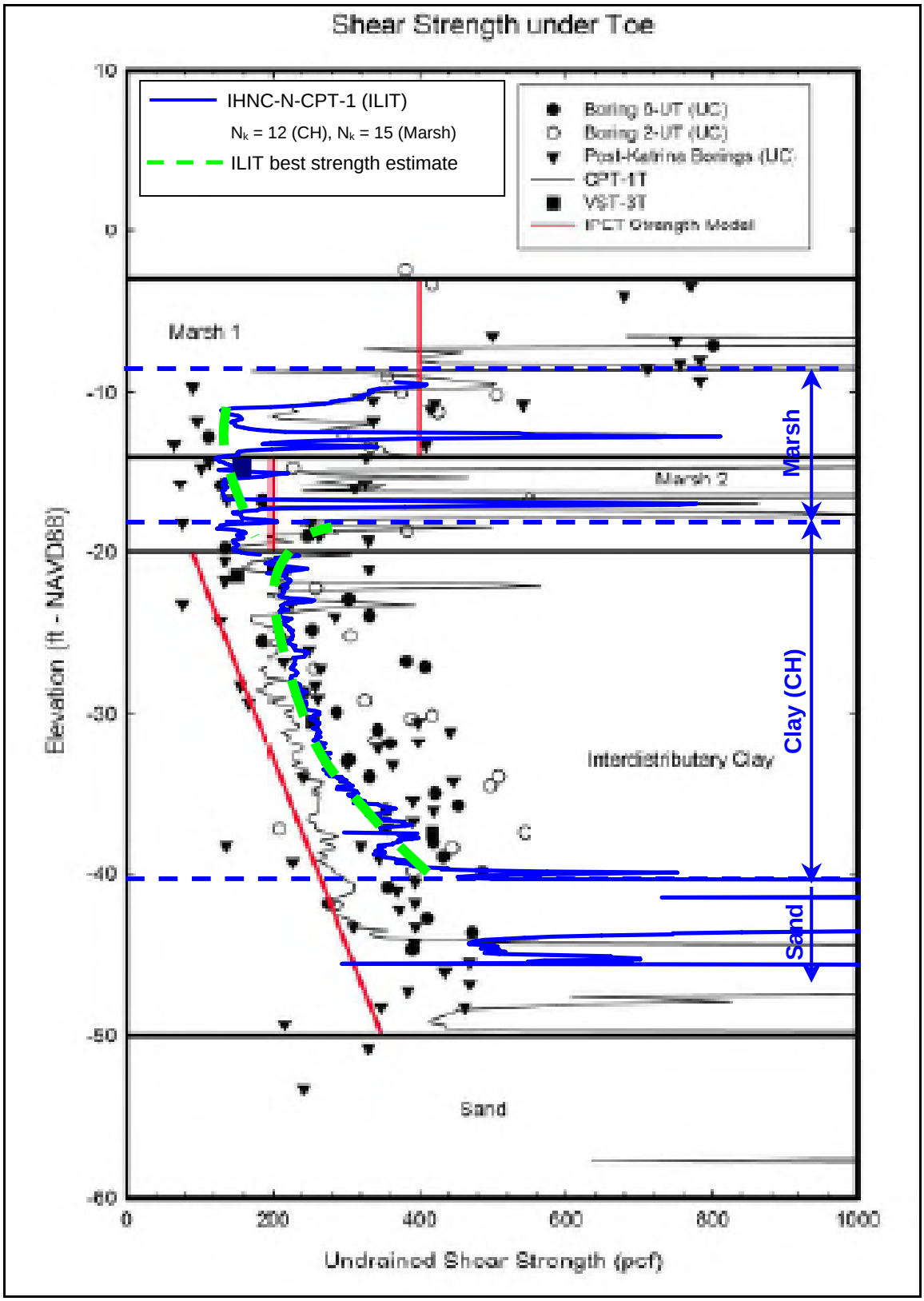

Figure 6.60: Re-interpretation of shear strength, and the ILIT shear strength profile.